Review

Literature Review on Thermodynamic and Kinetic Limitations of Thermal Decomposition of Methane

Andrzej Mianowski , Mateusz Szul * , Tomasz Radko , Aleksander Sobolewski , Tomasz Iluk

Posted Date: 1 August 2024

doi: 10.20944/preprints202408.0065.v1

Keywords: methane; thermo-catalytic decomposition; thermodynamics; kinetics; elementary reaction; KCE; EEC

 doi:10.20944/preprints202408.0065.v1

Review

Literature Review on Thermodynamic and Kinetic Limitations of Thermal Decomposition of Methane

Andrzej Mianowski, Mateusz Szul *, Tomasz Radko, Aleksander Sobolewski and Tomasz Iluk

Institute of Energy and Fuel Processing Technology (ITPE), Department of Circular Economy, Zamkowa 1, 41-803 Zabrze; Poland

* Correspondence: mszul@itpe.pl

Abstract: Based on literature data, an analysis was conducted on the thermodynamic and kinetic dependencies of the thermal decomposition of methane. Course of this process was analysed for both thermal and thermal-catalytic conditions. The elementary reaction, i.e. the synthesis of methane from its elements, including its reversibility, was used as the basis for the for considerations on the kinetic model. The conversion degree was adopted as the kinetic parameter (kinetic variable) since this measure is essential for determining the amount of carbon deposit formed and thus closing the mass balance of this process. Several different kinetic models for the elementary reaction were analysed to determine how do they relate in regard to the constant of the reaction rate. It was determined that regardless of whether the process is catalytic or purely thermal, for temperatures $t > 900$°C, the influence of reversibility of the reaction, has negligible influence on the yield of hydrogen produced, and thus can be omitted from the kinetic models. Special attention was given to iron-based catalysts, analysing the reactivity of Fe/C systems. It was demonstrated that the determined kinetic parameters satisfy the Kinetic Compensation Effect (KCE). Furthermore, by incorporating elements of Transition State Theory (TST), the existence of Entropy-Enthalpy Compensation (EEC) was highlighted. Based on these findings Authors show that through analysis of the changes in activation energy ($E = 20–421\ \mathrm{kJ \cdot mol^{-1}}$) only an estimate of the optimal process conditions can be found, because the isoconversional temperature is also dependent on the way in which the reaction is conducted ($T_{iso} = 1200 - 1450\ \mathrm{K} > T_{eq.}$). In other words, it was found that strong influences of such factors as *T, P,* etc. can locally compensate each other. Finally, it was also shown that the relations between KCE and EEC complement each other, which is confirmed by the determined average activation entropy at the isokinetic temperature ($\Delta S_B = -275.0\ \mathrm{J \cdot (mol \cdot K)^{-1}}$).

Keywords: methane; thermo-catalytic decomposition; thermodynamics; kinetics; elementary reaction; KCE; EEC

Introduction

Among known hydrocarbons from C_1 to C_{14}, methane is one of the most unreactive. It is characterized by the lowest Gibbs free energy, $\Delta_{298}\, G^{\emptyset} = -50.76\ \mathrm{kJ \cdot mol^{-1}}$ [1]. The situation changes when oxygen is introduced into the reaction system and in that case, at least six products must be considered, ranging from the most typical (CO_2, CO) to more complex coupling products such as C_2 hydrocarbons (ethane, ethene) or compounds containing oxygen functional groups (formaldehyde, methanol) [2].

Today's shift in the structure of consumption of energy commodities causes, among other things, intensification of the search for hydrogen production methods. This situation has led to interest in the process of methane pyrolysis, which is an endothermic ($\Delta_r\, H^{\emptyset} = 74.85\ \mathrm{kJ \cdot mol^{-1}}$) [3] thermal decomposition of methane that can be noted in the following manner:

$$\mathrm{CH_4} \rightleftarrows \mathrm{C} + 2\mathrm{H_2} \qquad (1)$$

The efficiency of reaction (1) can be influenced by changing process parameters such as temperature, pressure, as well as through the introduction of a catalyst. Another significant factor determining the course of reaction (1) is the method of heat supply. Generalization distinguishes

 doi:10.20944/preprints202408.0065.v1

indirect and direct supply of heat, but the type of reactor used can greatly influence the process. From the standpoint of reactor design, it is known that fixed bed, fluidized bed, or liquid bed reactor are most commonly applied. Moreover, when considering the temperature ranges >1300°C, or processes where plasma is used as a heat source for the reaction, the mechanism of reaction (1) can alter and other products besides hydrogen and structural carbon materials (carbon family) can be expected [3–5]. If reaction (1) is conducted at temperatures corresponding to the plasma state, upon quenching the resulting gaseous products, the following reactions may take place:

$$2CH_4 \rightleftarrows CH \equiv CH + 3H_2 \quad (2)$$

$$4CH_4 \rightleftarrows CH \equiv CH + CH_2 = CH_2 + 5H_2 \quad (3)$$

Thus, equation (1) should be regarded only as a conceptual/general notation of methane pyrolysis (thermal decomposition), while reactions (2) and (3) can illustrate examples of pathways for the formation of acetylene from methane. It should be noted that acetylene can also be obtained from methane through partial combustion, while the trimerization of acetylene is a pathway leading to the synthesis of benzene and higher aromatic hydrocarbons. The reaction network of methane with its pyrolysis products in the form of $C_{5\text{-}6}$ hydrocarbons is graphically presented in the work [6].

As it was already indicated the course and efficiency of reaction (1) can be influenced by many factors. One of the highest importance has the characteristics of the applied catalyst. In the work [7] most metals known for their activity for decomposition of methane were ranked in decreasing order of their impact on the efficiency/rate of reaction (1): Ni, Co, Ru, Rh > Pt, Re, Ir > Pd, Cu, W, Fe, Mo. Considering the cost criterion, it can be stated that the cheapest and most stable catalysts are those based on Ni, Co, and Fe. Belonging to the group of transition metals, these catalytic materials have partially filled 3d orbitals [7], which is an important similarity with catalysts used in industrial Fischer-Tropsch synthesis.

The above series left out one more catalyst, i.e. carbon materials exhibiting an ordered internal structure of the C element. Carbon catalysts finds somewhat lower attractiveness in pyrolysis of methane mainly due to the requirement for performing the process at temperatures higher than necessary for Fe or Ni (≥1000°C) and lower possibility for tailoring the quality of produced carbon structures. Equally for any type of catalyst available literature on this topic show that the deposition of carbon structures is the main reason for deactivation of the catalyst. Nevertheless, some forms of carbon deposits can be considered catalysts, thus theoretically making the process autocatalytic. Depending on the process conditions, including the characteristic of the catalyst used, carbon deposit produced in the reaction (1), consists of either one dominant or a mixture of different structural forms of the C element. Literature describes carbon black, mesoporous carbons, carbon nanotubes (CNTs), carbon nanofibers (CNFs), multi-walled carbon nanotubes (MWCNTs), amorphous turbostratic carbon, graphite-like carbon, filamentous (or foam) carbon as solid product of methane pyrolysis reaction. Collectively these materials are referred to as the "carbon family". Till this point there are no instances of classic allotropic forms of carbon being used in this place; however, activated carbons are. Two important pathways for purely thermal or utilizing carbon as catalyst in pyrolysis of methane need to be indicated here. First is connected with a somewhat novel approach where methane pyrolysis is performed to lower the reactivity of biochars (e.g. for metallurgical processes). In this application the reason for developing decomposing methane using biochar is to introduce the carbon deposits onto its surface, thus altering its structure In this case the structure of produced carbon deposits, or productivity of hydrogen play minor role. Second type of processes are those where tailoring and maintaining the quality of solid C-product is paramount. Today production of carbon black or graphite are the large-scale examples of the later. For the future though, we see the attention to shift towards structured carbon materials and also to hydrogen.

It is exactly due to the possibility of tailoring the properties of C-product why the literature on the selection of catalysts is so extensive. Among the catalysts listed above, nickel [3–5,7–47] holds a

 doi:10.20944/preprints202408.0065.v1

special position due to its effectiveness, while iron [3–5,7,8,27,31,40,42,48–61] is notable for being much cheaper and more environmentally friendly.

The characteristic that combines both iron and nickel in the context of reaction (1) is the multifunctional catalytic role of these materials, which is mainly attributed to the formation and decomposition of carbides. For this reason the processes associated with the carburisation and decarburisation of iron [62] deserve special attention. It is indicated that these processes involve the formation/decomposition reactions of cementite (Fe_3C) [60,63–67] as well as Hägg carbide (Fe_5C_2) [68]. Therefore in the context of iron, significant importance is attributed to the reactivity and properties of cementite [68–73]. In contrast, the literature is much poorer in research that considers the activity of nickel carbides Ni_3C, Ni_8C [13,45], or Ni_8C on TiC substrate [47].

When considering the course of catalysed reaction (1), the emergence of a new solid phase induces much higher level of complexity of the analysis. For pyrolysis, according to [4] the mechanism of molecular or dissociative adsorption on catalysts involves the formation of radicals: $CH_3^{\bullet}$, $CH_2^{\bullet}$, $CH^{\bullet}$, $C^{\bullet}$, $H^{\bullet}$ as well as their subsequent reduction and recombination. Final steps of these models are the nucleation of free carbon and the growth of its deposit [5]. It is generally accepted that the radical mechanism predominates for the reaction performed at temperatures >1200°C [41], and more details on reaction mechanisms can be found in [7,12,65,74–79].

Aim of the Work

In light of the above-presented information, in the subsequent parts of the review, Authors dispute the issues of phenomenological thermodynamics that were found to be inadequately described till this point.

In connection with the limitations presented in the literature regarding the comprehensive and unambiguous description of methane pyrolysis within a single model that represents its course on a micro scale, it was deemed appropriate to attempt an analysis of the validity of using an approach typical of phenomenological thermodynamics for this purpose. Therefore, in the subsequent part of this work, the applicability of kinetic equations as tools for describing the course of reaction (1) was verified, and thus the correctness of using the concept of an elementary reaction in the context of the methane pyrolysis process. To test the hypothesis that the constraints (limits) resulting solely from phenomenological thermodynamics are sufficient for verifying the above considerations, the study employed experimental results presented in the literature to date. It is important to note that in the analysed approach, the characteristic parameters are the Kinetic Compensation Effect (KCE) and the equivalent elements of Transition State Theory (TST) expressed through Entropy-Enthalpy Compensation (EEC).

Phenomenological Thermodynamics and Thermodynamics of Activation

From a thermodynamic point of view reaction (1) is reversible, and is expressed by the equilibrium constant that is a dependant of temperature and pressure and can be written as [3,4]:

$$K = K_p \left(\frac{P^{\emptyset}}{P}\right)^{\Delta\nu} \quad (4)$$

For reaction (1) and gaseous components $\Delta\nu = 1$.

Because this form of equilibrium constant description is of low utility, it is more valuable to derive this relationship using the Gibbs free energy of the process as a function of temperature. For Equation (1) such expression was presented e.g. in the work [20]:

$$\Delta rG\emptyset = 89.66 - 0.1023 \cdot T - 4.28 \cdot 10 - 6T2 - 2499.36T \text{ , kJ·mol}^{-1} \quad (5)$$

and through dividing both sides by $(-RT)$ we get:

 doi:10.20944/preprints202408.0065.v1

$$\ln K_p = -\frac{10784.08}{T} + 12.30 + 0.000515 \cdot T + \frac{300620.52}{T^2} \quad (6)$$

For the temperature $T_{eq.} = 818.84\ K$ above equations fulfil the criteria $\Delta G^{\emptyset} = 0$ and $K_p = 1$.

A modified, shorter version of the equation (5) can be expressed in the form that uses the relationship given in [55].

$$\Delta_r G^{\emptyset} = 88.039 - 0.1079 \cdot T,\ \text{kJ·mol}^{-1} \quad (7)$$

Similarly, this equation when divided by $(-RT)$ takes the form of:

$$\ln K_p = -\frac{10589.25}{T} + 12.978 \quad (8)$$

In Equation (8) similar constants are applicable: $573\ \text{K} \leq T_{eq} \leq 1773\ \text{K}$, $P = 0.1\ \text{MPa}$ and $T_{eq} = 815.93\ \text{K}$. When considering the above-mentioned constants a very similar relationship can be derived from [80] and for this reason Eqs. (4–8), and in particular Eqs. (7,8) are used as basis for further discussion.

On the other hand, algebraic forms of thermodynamic equilibrium constants $K = K_p = K_x = K_\alpha$ etc. (for constant total pressure) are correct for the following experimental (without subscript) and equilibrium (with the index *eq.*) values.

$$K = K_x = \left.\frac{{x_{H_2}}^2}{1 - x_{H_2}}\right|_{eq.} = \left.\frac{(1 - x_{CH_4})^2}{x_{CH_4}}\right|_{eq.} \quad (9)$$

Or

$$K = K_\alpha = \left.\frac{4{\alpha_{CH_4}}^2}{1 - {\alpha_{CH_4}}^2}\right|_{eq.} \quad (10)$$

for the condition of constant flow of methane $\dot{V} > 0$:

$$\alpha_{CH_4} = \frac{x_{H_2}}{2 - x_{H_2}} = \frac{1 - x_{CH_4}}{1 + x_{CH_4}} \quad (11)$$

Because

$$x_{H_2} + x_{CH_4} \equiv 1 \quad (12)$$

Similarly, the relations (11) and (12) are also correct for both experimental and equilibrium data derived from thermodynamic equations.

More in-depth thermodynamic considerations on reaction (1), taking into account also its mechanism, can be found in the following works [11,13,42,65,74,78,81–84] and the following Table 1 collates stoichiometric reactions and equations for Gibbs free energy for Eq. 1.

Phenomenological thermodynamics only reveals constraints arising from the equilibrium states of reaction (1). Because the course of this reaction can be promoted by the use of catalysts, the thermal decomposition process of methane must be analysed in the context of the reactions and transformations taking place on the catalyst and thus taking into account the interactions between the components of the reaction (1) and the catalyst. In the case of iron catalysts, special attention should be paid to iron ores, reason being that their choice is mainly attributed to good balance between optimal temperature of the process, low cost and quality of produced carbon structure. In further considerations the following minerals are of main interests: hematite, magnetite, goethite, and siderite. Despite physical differences of these minerals, the activity of iron catalysts can typically be described by comparing the observed effects of a given catalyst to the effects of the equivalent oxide form of hematite (Fe_2O_3) or the reduced form $\alpha - Fe$ [85].

In a strongly reducing atmosphere, a series of reduction reactions is observed, dependent on the temperature and the quality of the reductant [40,73,85–88]:

 doi:10.20944/preprints202408.0065.v1

$$Fe_2O_3 \rightarrow Fe_2O_3 \cdot FeO \rightarrow Fe_xO, \qquad \text{where } x = 0.82 \div 0.95 \xrightarrow[>575°C]{} FeO \xrightarrow[<912°C]{} \alpha - Fe \qquad (13)$$

In an atmosphere of diluted methane, hematite is reduced to wüstite (Fe_xO) at a much greater rate than in the subsequent phases of the reduction process to Fe [87], This process occurs according to two parallel mechanisms [88] and as the reduction of FeO is very slow, the same phenomena can also be observed in the case of hydrogen reduction. Comparative studies for the mentioned two iron oxides with respect to methane are justified due to the varying reaction rates [40].

Allotropic forms of iron are stable within specific temperature ranges [85]:

$$\alpha - Fe < 912°C, \qquad \gamma - Fe\ 912–1394°C, \qquad \alpha(\delta) - Fe\ 1394–1538°C \qquad (14)$$

where δ signifies the reformation of $\alpha - Fe$ with a body-centred cubic (BCC) structure, having a lattice size larger than that of $\alpha - Fe$. In contrast, $\gamma - Fe$ is characterized by a face-centred cubic (FCC) structure.

A comparison of the heat capacity for the polymorphic transformation $\alpha - Fe \rightarrow \gamma - Fe$ is presented in Figure 1. The maximum of the blue curve indicates the Curie point $T = 1042$ K. After integration and recalculation to the unit of $kJ \cdot mol^{-1}$, for the temperature range of $700–1300$ K, the following relation can be used
$G^{\emptyset} = -0.070 \cdot T + 19.65$. The linear characteristic of $\gamma - Fe$ disappears at the melting temperature of iron.

Experimental data used in the review were extracted from figures presented in the literature using software for digitalization of charts; e.g. https://plotdigitizer.com/.

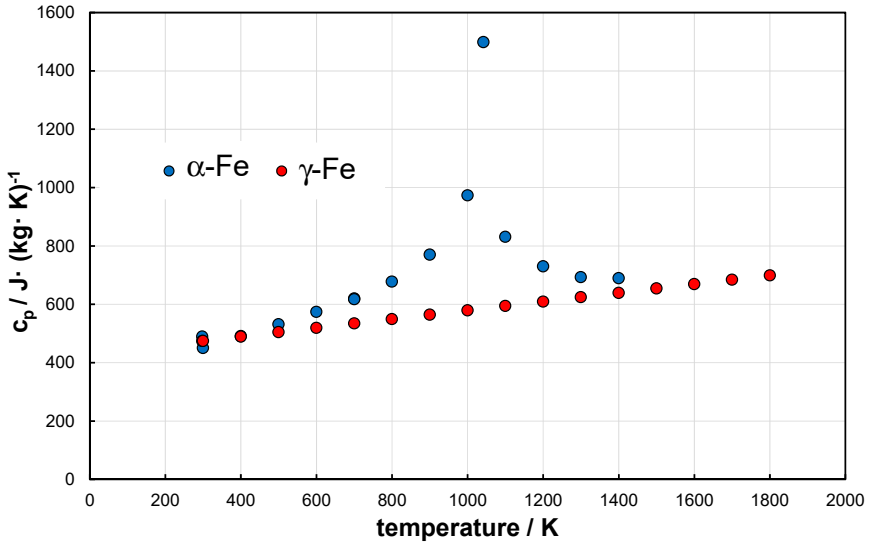

Figure 1. Change in heat capacity of $\alpha - Fe$ and $\gamma - Fe$ vs. temperature.

For $\alpha - Fe$, the polymorphic transformation is endothermic, and occurs within the temperature range $1000–1200$ K. Its value is $\Delta H^{\emptyset} = 10.29\ kJ \cdot mol^{-1}$
$= 184.24\ kJ \cdot kg^{-1}$. For reference the standard enthalpy for the decomposition reaction of methane without using a catalyst is $\Delta H^{\emptyset} = 74.85\ kJ \cdot mol^{-1}$.

In similar fashion to the data gathered for Equation (1), the following Table 1 collates also multiple correlations for possible polymorphic transformations of iron. E.g. position No 7 presents the value of free energy of the transformation $\alpha - Fe \rightarrow \gamma - Fe$ which was determined based on the data provided by the NIST [85]. Moreover, positions No 2–4 refer to the reaction of iron (III) oxide with methane according to the equations given in [59], while positions No 5–6 are associated with the formation and decomposition of iron carbides (primarily cementite). Analytical approaches to carburization and decarburization reactions of iron were presented by Grabke [62]. The diffusion

 doi:10.20944/preprints202408.0065.v1

coefficients of carbon into iron up to 912°C follow the sequence: $\alpha - Fe > \gamma - Fe \gg Fe_5C_2$ [68]. Interestingly for the reaction of FeO with methane, within the temperature range of 700–1100/1200 K, the thermodynamic existence of the Fe_3C phase was determined [89], while in works [66,69,72], the formation of cementite on active intermediate phase e.g. on hypereutectoid steels [72] and on orthorhombic crystal structure [60].

The formation of cementite is an endothermic reaction, meaning its decomposition is accompanied by an exothermic effect. Therefore, for methane decomposition processes conducted under isothermal conditions, knowledge of the temperature alone is inadequate, while taking into account the complete heat balance is crucial. Moreover, when using iron oxide catalysts, one must consider the formation of CO_2, CO, and water. For this reason, Table 1 collates also possible pathways where these species are present in the atmosphere of the process (No 6–12).

Table 1. Compilation of chemical reactions of species present in the atmosphere of methane pyrolysis process, including polymorphic transformation of iron, and their subsequent parameters of the Gibbs free energy equations: $\Delta_r G = a + bT$, $\mathrm{kJ \cdot mol^{-1}}$ P = 0.1 MPa.

No.	reaction	a, kJ·mol^{-1}	b, kJ·(mol·K)$^{-1}$	T range, K	T_{eq} for $\Delta_r G$ = 0, K	source	remarks
1	$CH_4 \rightleftarrows C + 2H_2$	88.04	−0.108	573–1773	815.2	[56]	Equation (7)
2	$2Fe_2O_3 + 3CH_4 \rightleftarrows 6H_2 + 3CO_2 + 4Fe$	248.37	−0.289	298–1300	859.4	[1]*	[59]
3	$Fe_2O_3 + 3CH_4 \rightleftarrows 6H_2 + 3CO + 2Fe$	252.16	−0.285	298–1300	884.8	[1]*	[59]
4	$2Fe_2O_3 + 3CH_4 \rightleftarrows 6H_2O + 3C + 4Fe$	158.12	−0.188	298–1300	841.1	[1]*	[59]
5	$3\alpha\text{-Fe} + C \rightleftarrows Fe_3C$	11.98	−0.017	700–1300	704.7	[1]*	analytical solutions for $\alpha - Fe$, graphite, Fe_3C given in [70]
6a	$3\alpha\text{-Fe} + CH_4 \rightleftarrows Fe_3C + 2H_2$	101.29	−0.122	773–1273	810.4	[1]	for Fe_3C assumed after [1] for
6b	$3\gamma\text{-Fe} + CH_4 \rightleftarrows Fe_3C + 2H_2$	101.29	−0.126	773–1273	804.0	[1]	485 <T< 1300K
7	$\alpha\text{-Fe} \rightarrow \gamma\text{-Fe}$	22.41	−0.066	700–1300	339.5	[85]	-
8	$CO + H_2O \rightleftarrows CO_2 + H_2$	−38.06	0.036	298–1300	1057.2	[1]	Water-Gas-Shift (WGS) [90–92] and
9	$H_2 + CO_2 \rightleftarrows CO + H_2O$	38.06	−0.036	298–1300	1057.2	[1]	Reverse-WGS [90–92]
10	$4H_2 + CO_2 \rightleftarrows CH_4 + 2H_2O$	−179.56	0.210	298–1300	855.0	[1]	R-WGS as methanation [91,93] Sabatier reaction
11	$C + H_2O \rightleftarrows CO + H_2$	137.20	−0.156	298–1300, 700–1300 for C	879.5	[1]	WG [4]
12	$C + CO_2 \rightleftarrows 2CO$	172.77	−0.169	298–1400	1022.3	[94]	Bell-Boudouard reaction

* polymorfic phase change No 7 was assumed.

doi:10.20944/preprints202408.0065.v1

 doi:10.20944/preprints202408.0065.v1

Furthermore, the linear dependencies obtained for the reactions presented in Table 1 were presented below in Figure 2. Within the temperature range considered for the methane pyrolysis process catalysed using iron catalysts, the homogeneous gas-phase reactions such as WGS (No 8), R-WGS (No 9), and methanation (No 10) were omitted. Reason for omitting WGS reaction (No 8) is the fact that it can be effectively conducted even at temperatures < 500°C. For the methanation reaction (No 10), where $\Delta_r G > 0$, a stoichiometric amount of hydrogen is required, specifically $H_2{:}\,CO_2 = 4{:}\,1$ [90,93].

Additionally, especially at temperatures exceeding 950°C the presence of methane in the reaction space counteracts methanation.

Finally, at $T > T_{eq.} = 1091\text{K}\,(818°\text{C})$, $\Delta_r G$ of the R-WGS reaction (No 9) is < 0, and the equilibrium conversion of CO_2 is > 0.5 [91]. Main reason though is the fact that R-WGS is conducted at lower temperatures and requires a bimetallic catalyst [90,91,93]. The course of the R-WGS reaction arises from the parallel existence of mechanisms involving the reduction of CO_2 to CO (through $COOH^{\bullet}$ synthesis and decomposition), as well as the oxidation of H_2 to H_2O [91]. Similarly to reactions No 8–10, the reactions No 11–12 were also omitted from Figure 2 because their occurrence is highly unlikely due to the lack of new gas-phase products.

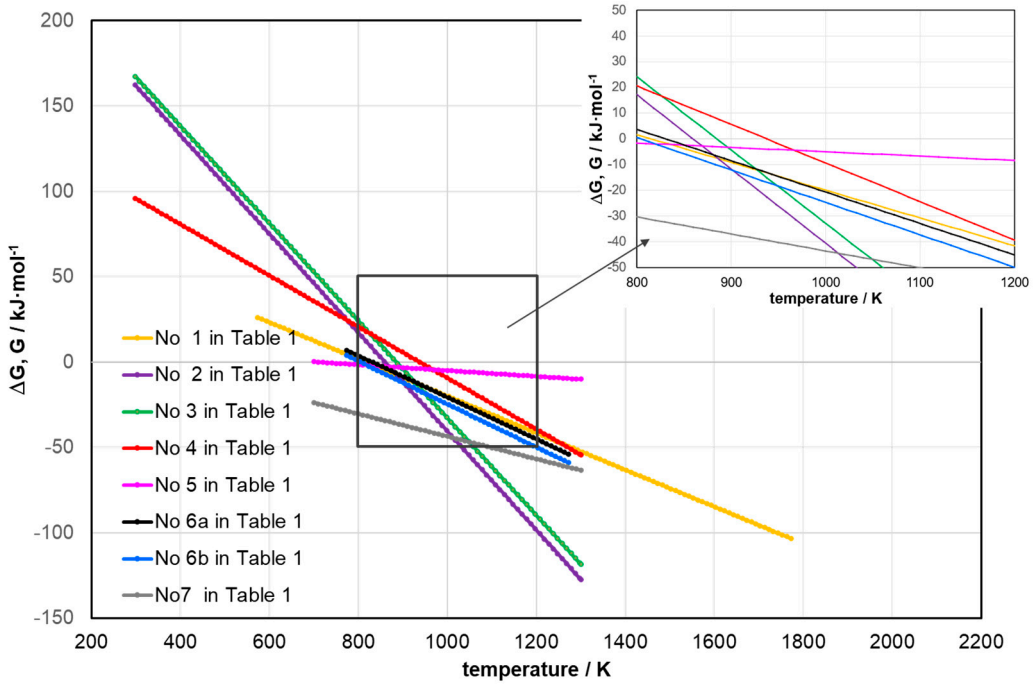

Figure 2. The dependence of free energy on temperature for reactions No 1–7 (Table 1).

For reaction (1) the most probable mechanism suggests that reactions occur on the catalyst surface, particularly through the reaction involving carbon bonding with iron, and in particular the formation of cementite due to carbon diffusion into the iron phase [68], which is the exact reason for catalytic properties of iron [4]. Examining the position of the equilibrium temperature ($T_{eq.}$), it can also be observed that iron oxides shift the equilibrium to the right, while metallic iron shifts it slightly to the left. An extreme example of methane decomposition is presented by reaction No 4 in Table 1. Here hydrogen is oxidized to water, which is one of the least expected variants of methane decomposition [59].

Modelling of the Forward and Backward Reactions

Utilising the phenomenological thermodynamics and in particular model of the first-order kinetics, the equilibrium constant can be expressed in the following logarithmic form:

 doi:10.20944/preprints202408.0065.v1

$$\ln K = \ln k_1 - \ln k_{-1} \tag{15}$$

After multiplication by $(-\mathrm{R}T)$ and using the relation that free energy of a reaction can be expressed as a difference in activation energies of the forwards and the backwards reactions [95] we can write that:

$$\Delta_r G^{\emptyset} = \Delta G^{+} - \Delta_{-1} G^{+} \tag{16}$$

each component of the right side of Equation (16) results from the comparison of Arrhenius kinetic constants with Eyring's TST [96]. Therefore, using the concept presented in [97] we obtain:

$$\Delta G^{+} = \mathrm{R} \cdot T \ln \frac{BT}{k_1} \text{ and } \Delta_{-1} G^{+} = \mathrm{R} \cdot T \ln \frac{BT}{k_{-1}} \tag{17}$$

Substitution of Equation (17) to Equation (16) leads to the following, convenient for calculations, form of equation:

$$\Delta_r G^{\emptyset} = \mathrm{R} \cdot T \ln \frac{k_{-1}}{k_1} \tag{18}$$

Variant 1 – from carburization of iron to methane decomposition on iron surface

According to [62] aforementioned processes of carburisation and decarburisation of iron are based on isothermal reactions performed in the temperature range 800–1040°C. In the original text, Authors use the following notation:

$$\mathrm{C}\,(\mathrm{in}\,\gamma - \mathrm{Fe}) + 2\mathrm{H_2(g)} \leftrightarrow \mathrm{CH_4(g)} \tag{19}$$

Enthalpy of this reaction was determined to be $\Delta_r H^{\emptyset} = -124.3$ kJ·mol^{-1}.

Grabke [62] has determined the rate constants for the reaction (19); however, the notation adapted in this work is incoherent with units used herein. In the following considerations the reverse direction of the reaction (19) is used, i.e. from right to the left. Moreover, by unifying the dimensions to the scale s^{-1} we obtain that for the reaction of methane decomposition:

$$k_1 = 4.55 \cdot 10^3 \left[\exp\left(-\frac{230120}{\mathrm{R}T}\right)\right],$$

while for the reaction of methane synthesis (Equation (19) as given above, i.e. from left to right):

$$k_{-1} = 2.6 \cdot 10^{-2} \left[\exp\left(-\frac{105860}{\mathrm{R}T}\right)\right]$$

In this way according to Equation (18) we obtain:

$$\Delta_r G^{\emptyset} = 124.27 - 0.100T \tag{20}$$

Interestingly, thus obtained parameters of the Equation (20) are close to the values given in reaction No 6b in Table 1. For $\mathrm{Fe_3C}$ the slightly higher value of the intercept can be explained by the nonlinear relation between free energy and temperature [70], which in simplistic approach for range of 298.15–1500 K, can be approximated by a second degree parabolic function [1,60]. For smaller temperature ranges the polynomial can be reduced to linear form, and thus the values of the intercept can be determined to change in the range 70–116 kJ·mol^{-1}. On the other hand when accepting after [60] the range of 500–2000 K, the relationship No 6b adapts the following form having much higher values of the constants $\Delta_r G^{\emptyset} = 126.27 - 0.144 \cdot T$. Thus, the above expression of Equation (20) correlates well with the reaction of methane decomposition in the presence of metallic iron catalyst ($\gamma - \mathrm{Fe}$). Unfortunately, in [60] Authors do not specify to what extend it is possible to treat the solution of $\gamma - \mathrm{Fe}$ and C as cementite.

Finally, returning to the notation of Equation (19) the above considerations indicate correctness of the approach where decomposition of methane is analysed in the categories of Eyring's TST [96].For this scope the above statement underlines the first principles of reaction (1) noted in [7].

 doi:10.20944/preprints202408.0065.v1

Variant 2 – Free Energy of Activation of the Reaction (1)

The above analysis shows the link between works carried out to develop carburization/decarburization process, in the light of methane pyrolysis though it is important to counterpose this analysis with the general scheme of the methane pyrolysis reaction (1).

Similarly to the previous case, in the following example two different sources of kinetic data were analysed for their convergence using Equation (16). In formal terms here the value of the component ΔG^+ is sought, thus the notification of Equation (16) changes to:

$$\Delta G^+ = \Delta_r G^{\emptyset} + \Delta_{-1} G^+ \tag{21}$$

Based on kinetic data reduced to the form of Arrhenius equation and describing a high-temperature (1080–3000°C) and high-pressure (up to 5.61 MPa) methane synthesis process of hydrogen attacking graphitic materials, the following kinetic parameters were determined: $A = 5.9\ \mathrm{s}^{-1}$, $E = 101.50\ \mathrm{kJ \cdot mol^{-1}}$ [98]. For the temperature range of 500–1500 K, these data result in the following expression of the free energy of activation:

$$\Delta_{-1} G^+ = 93.88 + 0.248 \cdot T \tag{22}$$

for the reaction No 1 in Table 1, after considering Equation (22), we obtain:

$$\Delta G^+ = 181.92 + 0.140 \cdot T \tag{23}$$

The literature presents great efforts made to find suitable data consistent with the existing dataset, especially one enabling the comparison of determined kinetic and thermodynamic parameters. In [55], Authors have determined and utilised data describing the kinetics of methane decomposition using a graphite crucible and liquid slag having a predominant content of CaO (43% by mass) and only a minimal content of FeO (0.37% by mass). This work provides the following parameters, $A = 4.053\ 10^6\ \mathrm{cm^{-1} \cdot s^{-1}}$, $E = 190.31\ \mathrm{kJ \cdot mol^{-1}}$ and on this premiss the following can be determined:

$$\Delta G^+ = 182.69 + 0.130 \cdot T \tag{24a}$$

Then, after correcting to the form $A = 4.819 \cdot 10^7\ \mathrm{s^{-1}}$ we obtain:

$$\Delta G^+ = 181.41 + 0.120 \cdot T \tag{24b}$$

which yet again is similar to the coefficients determined beforehand. Moreover, when comparing kinetic parameters, the issue of dimensional consistency for the frequency factor A is debatable. It is simplest to assume it represents the "directional vector of path of reaction scaled by reciprocal time". Similar interpretations are sometimes applied, albeit for different types of variability [93].

Comparison of the coefficients given in Eqs. (23) and (24a,b) indicates good convergence for the two presented above routes for analysing the process of methane decomposition using iron catalyst.

Moreover, despite the fact that the objectives of references [62,98] are related to iron metallurgy, and therefore not directly aligned with the main scope of this study, based on the kinetic data provided in the, it is possible to consider the solid solution of $\mathrm{Fe + C}$ (wüstite) as a catalyst for methane decomposition.

Kinetics – Introduction

Above thermodynamic considerations concerning equations Eqs. (15,16) and Equation (21), already took advantage of kinetic parameters determined by using the Arrhenius law. These deliberations also underscore the validity of analysing kinetic equations that include the equilibrium constant.

In the context of kinetics the literature on methane pyrolysis encompass such variables as: methane and hydrogen mole fractions, their partial pressures, methane conversion rate, as well as

 doi:10.20944/preprints202408.0065.v1

the rate (or quantity) of carbon formation per unit of catalyst mass – expressed respectively in [g or $\text{mol} \cdot \text{g}_{\text{cat}}^{-1} \cdot \text{unit of time}^{-1}$] or [g or $\text{mol} \cdot \text{g}_{\text{cat}}^{-1}$]. The link between the amount of carbon deposit formed stems from a volumetric balance for $\dot{V} = \text{const.}$, typically having the unit of [dm^3 or $\text{m}^3 \cdot \text{g}_{\text{cat}}^{-1} \cdot \text{unit of time}^{-1}$]. For further considerations it needs to be pointed out that due to its practical nature conversion degree should be regarded with particular importance. In an integrated approach, following [27,58], the quantity of carbon deposition can be expressed in terms of conversion degree:

$$[C] = \frac{12}{22.4}\dot{V}\int_0^t \alpha \, \mathrm{d}t \tag{25}$$

Literature presents also the following expression as the second way of modelling the kinetics of the deposition of carbon [35,39,42,99–101]:

$$r_C = \frac{\mathrm{d}[C]}{\mathrm{d}t} = k(P_{\mathrm{CH_4}})^n, \; n = 0.5 \div 1, \tag{26}$$

In this approach r_C can be understood as the initial rate of formation of the carbon deposit, with only one variable remaining (here $P_{\mathrm{CH_4}}$).

From the description of research presented in [100], it stems that $\frac{P_{\mathrm{CH_4}}}{P^{\emptyset}} = x_0 = \text{const}$ for a singular carrier of methane, but $x_0 = \text{var}$ for several different streams.

Furthermore, in works [14,83] Equation (26) was used to indicate the existence of a maximum rate of formation of the carbon deposit, and this results from the activity of the catalyst used. Once the maximum is reached, a decrease in the productivity of the deposit is observed; hence as indicated in [102], the formation of carbon deposits can also be expressed empirically as a function of time:

$$[C] \propto t^n, \qquad \mathrm{n} < 1 \tag{27}$$

Better understanding of this relation can be gained after substituting the simplest linear relationship for the conversion degree vs. time into Equation (25). Upon integration, the relationship between the amount of deposit formed over time takes the form of a second-degree parabolic equation. Another way to represent Equation (25) is to replace the integral with the average conversion degree:

$$[C] = \frac{12}{22{,}4}\dot{V}\bar{\alpha}t \tag{28}$$

In the following Table 2, selected literature data are compared to indicate the amount of carbon deposit formed in the process of fluidised-bed methane pyrolysis at temperatures of 650–800°C using $NiCu/Al_2O_3$ catalyst and with $WHSV = 12 \; \text{L} \cdot \text{g}_{\text{cat}}^{-1} \cdot \text{h}^{-1}$.

Table 2. Comparison of experimental data for fluidized bed pyrolysis of methane where $NiCu/Al_2O_3$ was used as catalyst.

Temperature in °C; model for H_2	**$\bar{\alpha}$, calculated as an average value of an integral**	**$[C]$, $\text{g} \cdot \text{g}_{\text{cat}}^{-1}$ calculated from Equation (28)**	**$[C]$,$\cdot \text{g} \cdot \text{g}_{\text{cat}}^{-1}$ in [27] (time of the process in minutes)**
650; exponential	0.127	5.71	4.97 (420)
700; linear	0.404	18.17	18.41 (420)
750; exponential	0.288	12.95	12.95 (420)
800; exponential	0.303	8.44	8.80 (300)

The second column of Table 2 presents the calculated integral mean for methane conversion, integrating from time $t = 0$, when the point of maximum conversion is achieved, up to the end of the experiment (finite time). The third and fourth columns show respectively the amounts of carbon deposit calculated using equation (28) and the experimental quantities of deposit reported in [27]. The calculations pertain to the methane pyrolysis stage during catalyst deactivation, excluding the progress of the elementary reaction.

 doi:10.20944/preprints202408.0065.v1

Literature descriptions of methane pyrolysis processes indicate that there are two steps that need to be considered. During the initial step, methane conversion, carbon deposition, and hydrogen content in the process gas increase, while the methane concentration decreases. This period can be understood as activation step. During the second period of the process, after time $t \geq \tau_D$, where τ_D is the deactivation time, an ongoing process of deactivation of the catalyst is observed [103]:

$$r(t) = r_0 \exp\left(-\frac{t}{\tau_D}\right), \text{for } t = 0, r(t) = r_0 \tag{29}$$

Following after Becker [104] that expressions for reaction rate do not take into account the backwards reaction, for the molar fraction of methane, we obtain:

$$r = -\frac{\mathrm{d}x_{\mathrm{CH_4}}}{\mathrm{d}t} = k_1 (x_{\mathrm{CH_4}})^n, \qquad n = 1 \div 1.5 \tag{30}$$

Similar expression for reaction rate is also proposed by other authors [105].

Given the considerations outlined above, we need to ask how the concept of an elementary reaction is understood.

Kinetics of the Elemental Reaction Equation (1)

In Gold Book the elemental reaction is defined in the following way [106]: "A reaction for which no reaction intermediates have been detected or need to be postulated in order to describe the chemical reaction on a molecular scale. An elementary reaction is assumed to occur in a single step and to pass through a single transition state."

In practice quoted description can be narrowed down to the complete conversion state of substrates according to the stoichiometric expression or to a limited equilibrium state.

For reaction (1) equilibrium constant is determined from the relation characteristic for the first order kinetics (see Equation (15)):

$$K = \frac{k_1}{k_{-1}} \tag{31}$$

and its rate can be expressed in the following form:

$$r = k_1 x - k_{-1}(1-x)^2, \qquad T = \text{const} \tag{32}$$

where:

$$r = -\frac{\mathrm{d}x}{\mathrm{d}t} \tag{33}$$

Coupling the Eqs. (31-33) leads to the form of an equation having separate variables:

$$-\frac{\mathrm{d}x}{\mathrm{d}t} = k_1 \left[x - \frac{(1-x)^2}{K}\right] \tag{34}$$

In Eg(34) the equilibrium constant is expressed using formula (8) or (6).

Furthermore, in the work of [82] utilizing previous publication [107] the following initial condition was accepted x_0:

$$g(x) = k_1 t \tag{35}$$

while:

$$k_1 t = \frac{x_0 - x_{eq.}}{x_0 + x_{eq.}} \ln\left(\frac{x_0^2 - x \cdot x_{eq.}}{x_0 (x - x_{eq.})}\right) \tag{36}$$

and for $t = 0$, $x = x_0$ and $x < x_{eq.}$ (intercept = 0).

Importantly for further considerations this research was conducted in a manner most similar to the analysis of an elementary reaction, as it was performed in a semi batch system, where the inflow of methane was minimal, solely to maintain constant pressure, and the hydrogen concentration

 doi:10.20944/preprints202408.0065.v1

measurements were taken post-process. For constant temperatures ranged from 700°C to 900°C, and under total pressure of 2.82–5.61 MPa, the thus obtained results can be attributed to a gradient-free process.

By substituting into Equation (36) the relationship between the molar concentration of methane, from:

$$x = x_0 \frac{1-\alpha}{1+x_0\alpha} \tag{37}$$

the following solution that includes the kinetics in the form of the degree of methane conversion can be obtained:

$$k_1 t = \frac{\alpha_{eq.}(1+x_0)}{2-\alpha_{eq.}(1-x_0)} \cdot \ln\left(\frac{\alpha_{eq.}+\alpha-\alpha\cdot\alpha_{eq.}(1-x_0)}{\alpha_{eq.}-\alpha}\right) \tag{38}$$

For $x_0 = 1$ (pure methane) Equation (38) converts to the form:

$$k_1 t = \alpha_{eq.} \ln\left(\frac{\alpha_{eq.}+\alpha}{\alpha_{eq.}-\alpha}\right), \alpha_{eq.} > \alpha \tag{39}$$

Or

$$k_1 t = \alpha_{eq.} \ln\left(\frac{1+z}{1-z}\right), z < 1 \tag{40}$$

where $z = \frac{\alpha}{\alpha_{eq.}}$ is thermodynamic efficiency of reaction (1), and kinetic functions $g(\alpha)$ and $g(z)$ correspond to the notation of their complete kinetic forms ($= k_1 t$).

In Equation (40) for $t = 0$, $z = 0$, or when $t \to \infty$, $z \to 1$, and thus for small values of z, an approximate result can be sought through expansion to a series:

$$\ln\left(\frac{1+z}{1-z}\right) = 2\sum_{1}^{\infty}\left[\left(\frac{1}{2n-1}\right)z^{2n-1}\right], z^2 < 1 \tag{41}$$

Approximate solution to the above equation can be found through limiting it to the first term:

$$\ln\left(\frac{1+z}{1-z}\right) \cong 2z \tag{42}$$

Furthermore, by putting Equation (42) into Equation (40) one can describe a minimal operation line:

$$\alpha = \frac{k_1}{2} t = k_z t \tag{43}$$

As an example of the effectiveness of such procedure the following Figure 3. was introduced. It presents a transformation of results presented in [82,107] to the form of relation Equation (39), which was further simplified to linear relation of Equation (43). As a result, for the following conditions: $x_0 = 1$, methane flow $\dot{V} \approx 0$, then $\alpha = 1 - x$, the following results were obtained: $E = 130.5$ kJ·mol^{-1}; $\ln A = 8.60$ (A in s^{-1}). For reference acc. to [82,107] $E = 131.0$ kJ·mol^{-1}; and $\ln A = 8.59$ (A in s^{-1}).

 doi:10.20944/preprints202408.0065.v1

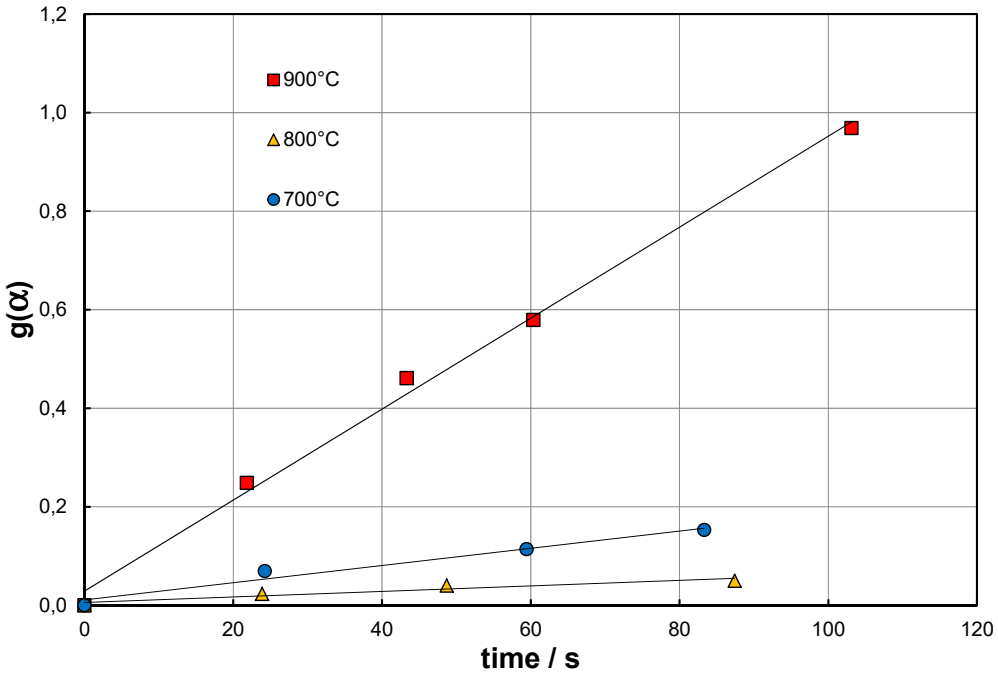

Figure 3. Transformation of the experimental results from [82,107] to the form of Equation (39) further simplified to linear relation of Equation (43).

The commentary on the data presented in Figure 3 can be summarized in a few remarks. By comparing the structure of equations Equation (36) and Equation (43), it is apparent that the kinetics of the process can be interpreted using multiple models of varying complexity. This is a fairly common observation in studies of heterogeneous systems involving both solid and gas phases. E.g. if Equation (34) is expressed in another form, say as:

$$-\frac{\mathrm{d}x}{\mathrm{d}t} = k_1 x \left[1 - \frac{(1-x)^2}{xK}\right] \tag{44}$$

and furthermore, by using Eqs. (4) and (9), the following can be written:

$$-\frac{\mathrm{d}x}{\mathrm{d}t} = k_1 x \left(1 - \frac{K_x}{K}\right) \tag{45}$$

When reaction (1) remains „very far" from equilibrium $(K \gg K_x)$ according to [107], for $\dot{V} = 0$ it follows first degree kinetics, and thus Equation (45) can be described by in the terms of conversion degree:

$$g(\alpha) = -\ln(1 - \alpha) = k_1 t\,, T = const \tag{46}$$

On the other hand, for small conversion degrees, reaction (1) has a zero-degree kinetics.

In kinetic considerations, it is usually deemed appropriate to adopt models with the least complexity while maintaining sufficient precision. The results of studies on the elementary reaction (1) under high pressure [82,107] indicate that the equilibrium state, represented by the equilibrium conversion degree, stands here as a limiting factor. The deviation from equilibrium influences the kinetics, which can be expressed through various modelling approaches, e.g. according to n^{th} or fractional order variability [104].

As it was already introduced, literature published in the topic of methane pyrolysis refer to the inequality $z = \frac{\alpha}{\alpha_{eq.}} < 1$ as a mean of describing the thermodynamic efficiency of the process, however, in certain process conditions, e.g. for some temperature ranges $z \approx 1$ [19,38] – for research published in [38] such a case has been noted only for the catalysts consisting of 50%Ni-10% Cu/Si0₂.

 doi:10.20944/preprints202408.0065.v1

Continuous process – conditions of constant flow of methane

For the sake of broadening the discussion to continuous flow systems, Equation (34) was solved for the flow condition, $\dot{V} > 0$. Differentiating the Equation (37) in respect to time reduces it to the expression for the rate of reaction (1), taking the following form:

$$-\frac{\mathrm{d}x}{\mathrm{d}t} = x_0(1+x_0)\cdot(1+x_0\alpha)^{-2}\frac{\mathrm{d}\alpha}{\mathrm{d}t} \tag{47}$$

and after substituting Eqs. (37), (47) as well as thermodynamic equilibrium constant (10) to Equation (34), when the condition $z = \frac{\alpha}{\alpha_{eq.}} < 1$ is fulfilled, we finally obtain the following kinetic expression for flow conditions related to the degree of methane conversion:

$$\frac{\mathrm{d}\alpha}{\mathrm{d}t} = k_1\frac{2-\alpha_{eq.}(1-x_0)}{\alpha_{eq.}(1+x_0)}\cdot\frac{(c\cdot\alpha+\alpha_{eq.})(\alpha_{eq.}-\alpha)}{\alpha_{eq.}(1+c)}\text{, where } c = 1-\alpha_{eq.}(1-x_0) \tag{48}$$

For initial condition $x_0 = 1$ (pure methane) the complicated Equation (48) reduces to a form which greatly simplifies kinetic interpretation:

$$\frac{\mathrm{d}\alpha}{\mathrm{d}t} = \frac{\mathrm{k}_1}{2}\left[1-\left(\frac{\alpha}{\alpha_{\mathrm{eq.}}}\right)^2\right], \qquad T = \text{const} \tag{49}$$

This otherwise can also be expressed it in terms of thermodynamic efficiency:

$$\frac{\mathrm{d}z}{\mathrm{d}t} = \frac{k_1}{2\alpha_{eq.}}(1-z^2) \tag{50}$$

Eqs. (49) and (50) indicate that under flow conditions of methane, the reaction rate is quasi second order, which is consistent with the exponent related to the hydrogen formation presented in Equation (32). Noteworthy, the considerations expressed in Eqs. (47–50) highlight the possibility of variable order of the reaction (1) depending on the conditions under which it is carried out.

The solution to Equation (50) is expressed in Equation (40). Looking at the form of Equation (40), a question arises, whether this expression is suitable for use in complex studies of reaction (1), especially where the presence of catalysts and its reactions with methane are taken into account (Table 1).

On the other hand, in Equation (38) for $(\alpha_{eq.} = 1), (x_0 < 1)$, after substitution and rearrangement, we obtain:

$$g(\alpha) = k_1 t = \ln\left(\frac{1+x_0\alpha}{1-\alpha}\right) \tag{51}$$

hence, for $t = 0$, $\alpha = 0$, and when $t \to \infty$, $\alpha \to 1$.

Solution of Equation (34) for $\boldsymbol{x_0 < 1}$ *and considering equilibrium constant* K

Due to the stoichiometry of reaction (1), methane diluted with inert gas is very often used as a feed in experiments. Taking into account the mass balance of (37), the equilibrium constant in its fractional form (Equation (10)) contains the initial molar fraction of methane $x_0 < 1$:

$$K = \frac{(1-x_0+2x_0\alpha_{eq.})^2}{x_0(1+x_0\alpha_{eq.})(1-\alpha_{eq.})} \tag{52}$$

From Equation (52) equilibrium conversion degree reduces to the following quadratic equation:

$$\alpha_{eq.}^2 + \frac{1-x_0}{x_0}\alpha_{eq.} + \frac{x_0^2 - x_0(2+K)+1}{x_0^2(4+K)} = 0 \tag{53}$$

From the above we know that for 50% dilution of methane with nitrogen $x_0 = 0.5$ and for temperature of $T = 1173\,\mathrm{K}$ from equation (8) we can calculate $K = K_p = 55.40$ from this the following expression can be written:

 doi:10.20944/preprints202408.0065.v1

$$\alpha_{eq.}^2 + \alpha_{eq.} - 1.848 = 0 \tag{54}$$

After solving we obtain $\alpha_{eq.} = 0.950 \cong 1$. This result allows the use of the kinetic equation (32) without the reversible term, i.e. setting $k_{-1} = 0$. In equation (54), for the rounded value of the intercept ($-1.848 \cong -2$), $\alpha_{eq.} \equiv 1$ and from equation (53) it is known that for the above-mentioned conditions, dilution of the methane stream $(x_0 < 1)$ and an increase in temperature $(K \to \infty)$ justify the conclusion that reaction (1) is irreversible.

Thus for $(k_{-1} = 0)$ combining Eqs (32), (33), (37) and (47) leads to a kinetic equation in terms of the methane conversion degree:

$$\frac{\mathrm{d}\alpha}{\mathrm{d}t} = \frac{k_1}{1 + x_0}(1 - \alpha)(1 + x_0\alpha), \qquad T = \text{const} \tag{55}$$

which solves Equation (51) and lead to constatation that for $x_0 = 1$ and (39) for $\alpha_{eq.} = 1$ are identical.

Analogous consideration for Equation (43) leads to the following expression:

$$\alpha = \frac{k_1}{1 + x_0}t = k_z t \tag{56}$$

Presented below Table 3 summarizes the integral forms of kinetic models. Importantly these equations relate to the following conditions: $\dot{V} > 0$, $x_0 < 1$, $\alpha \in [0; \alpha_{max}]$, $\alpha_{eq.} = 1$ and positions No 2–3 consider the catalytic process. For practical reasons it is important that these expressions feature the term $-\ln(1 - \alpha)$, which is characteristic of first-order kinetics. In further consideration this term is denoted by the symbol $(F1)$.

Table 3. Integral forms of $g(\alpha) = k_1 t$.

No	$\mathrm{d}\alpha/\mathrm{d}t =$	$g(\alpha) =$	remarks	sources
1	$\frac{k_1}{1 + x_0}(1 - \alpha)(1 + x_0\alpha)$	$\ln\left(\frac{1 + x_0\alpha}{1 - \alpha}\right)$	For $x_0 = 1$ $\mathrm{d}\alpha/\mathrm{d}t = \frac{k_1}{2}(1 - \alpha^2)$	Eqs. (51),(55)
2	$k_1\frac{1 - \alpha}{1 + \alpha}$	$-2\ln(1 - \alpha) - \alpha$	Proposed for analysis of reactivity of cokes towards CO_2; year 1955 [108]	Eq. proposed by Lee [101], model D–J
3	$k_1\frac{1 - \alpha}{1 + \varepsilon\alpha}$	$-(1 + \varepsilon)\ln(1 - \alpha) - \varepsilon\alpha$ $\varepsilon = 1/2$	ε in [101] as well as in [22,109] is defined in the form given by [110]. For system consisting of isomorphic spheres $\varepsilon = 1 - (\pi/6) = 0.476$	[22] (2004) and [109] (2016)
4	$\left(\frac{k_1}{\beta}\right)\frac{1 - \alpha}{1 + x_0\alpha}$	$-(1 + x_0)\beta\ln(1 - \alpha)$ $- x_0\beta\alpha$	Acc. to [111], β = 0.43–0.71	[111–113], for $\beta = 1$, $T =$ 1023– 1373 K, for three types of reactors [114,115]
5	$k_1(1 - \alpha)$	$-\ln(1 - \alpha)$	Here $\varepsilon = 0$ which acc. to [110] means constant density	Equation (46), model F1

The reaction rate presented in Table 3 indicates that the reaction order ranges from first-order kinetics (model F1, No 5) to quasi-second order (No 1 and 2). The process described in position No 4 is particularly interesting as it utilizes a solar heating system (solar reactor), and it is conducted without using a catalyst. Uniqueness of this process lies in the injection of methane into argon at high temperatures. The residence time in the reactor was calculated as a substitute time, which is the ratio

 doi:10.20944/preprints202408.0065.v1

of the reactor volume to the flow rate. The physical dilatation factor (β) [111–113] considers the relationship between the state parameters (temperature, pressure) at the reactor inlet and those under reaction conditions. Further explanations and implications of this approach are analysed in works [114,115]. Importantly in these works the calculated Arrhenius law parameters are similar in value to previous studies. Additionally, the analysis of the equations given in [114,115] and also presented in [111] indicates that the chemical expansion factor directly corresponds to the value described herein as (x_0). The results of the studies presented in [111–115] are thus significant enough to be considered as having primary importance. Finally, as a result of the considerations presented in Table 3 it can be noted that with $\varepsilon = 0$ the position No 5 and Equation (46) stand as the simplest kinetic model of the reaction (1), model (F1).

Comprehensive nature of the above presented considerations on the kinetic model of reaction (1) forms ground upon which experimental data can be analysed. Subsequent examples illustrate their validity in practical use.

Result of the first example is presented in Figure 4. Data for the analysis were extracted from the experimental research presented in [57]. Author proposed here the use of a specially prepared iron mesh to catalytically decompose methane. The pyrolysis was performed under $t = 800°C$, $x_0 = 1$; however, beforehand the catalyst was activated using hydrogen. Analysis of the dataset using the approach presented in Figure 3, which is pertinent to the elementary reaction only, gives unsatisfactory results because of the systematic deviations of the linear relationship. The deviations can be explained by the formation/decomposition of cementite. Followingly, further analysis of the data set shows that after approximately 20 hours, the catalyst becomes saturated with carbon. In the time interval of 25.42–35.09 hours (number of measurements $N = 20$) the results can be approximated by a linear relationship. In this way it is possible to determine the average reaction rate constant $k_1 = 4.20 \cdot 10^{-5}\,s^{-1}$, $g(\alpha) = 0.1512 \cdot t - 2.9254$ (t in hours) and $r^2 = 0.9891$. Model F1 (No 5 in Table 3) stands out from the rest as it characterizes a separate kinetic approach, which forms an independent correlation and demands to be fitted with additional, process related terms to adequately characterize reaction (1). The determined kinetic constant for F1 is ($k_1 = 2.69 \cdot 10^{-5}\,s^{-1}$) ($r^2 =$ 0.9882), and for the models for which it was determined, is close to half the value determined using Eqs. (43) and (56). Noteworthy fractional order models were not analysed here, even though they could be adequate.

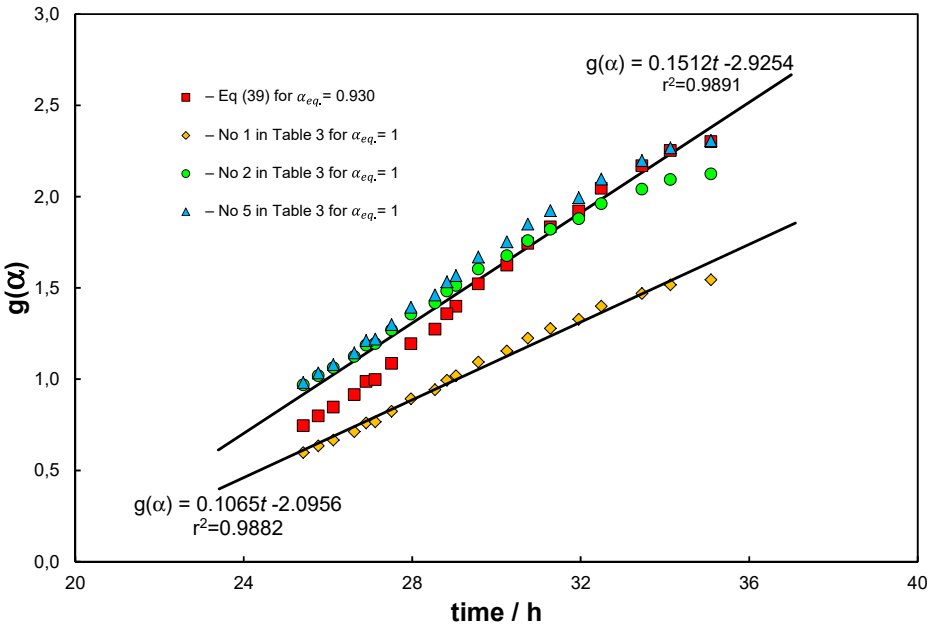

Figure 4. Graphical presentation of kinetic equations $\boldsymbol{g(\alpha) = k_1 t}$ for data showed in [57]

The above figure presents very small conversion degree. This suggests the greatest distance from equilibrium (DFE), which under extreme conditions:

 doi:10.20944/preprints202408.0065.v1

$DFE = 1 - z$, for $\alpha = 0,\ z = 0,\ DEF = 1$ and for $\alpha = \alpha_{eq.},\ DFE = 0$ (57)

The concept of Distance From Equilibrium (DFE) exists in the literature, but its formal representations vary [116,117]. The basic, definitional expression of DFE is represented by the term given in parentheses in Equation (45), $(1 - K_x/K)$, whereas Equation (57) provides a justified measure of DFE in a geometric sense.

A separate issue is the conversion degree achieved near the deactivation of the catalyst $(\alpha_{max} \leq \alpha_{eq.})$. An example of this problem is illustrated in Figure 5, where experimental data from the study [38], after recalculation using Equation (51), illustrate the kinetics of the final stage of catalytic activation and a sharp transition to the kinetics of catalytic deactivation. This transition is associated with the inversion of the slope coefficient through the appearance of a sign change.

It is worth noting here that in this research the methane stream fed into the reactor was diluted with nitrogen in a 1:1 ratio ($x_0 = 0.5$), the process was run at $t = 750°C$, as well as $\alpha_{eq.} = 1$.

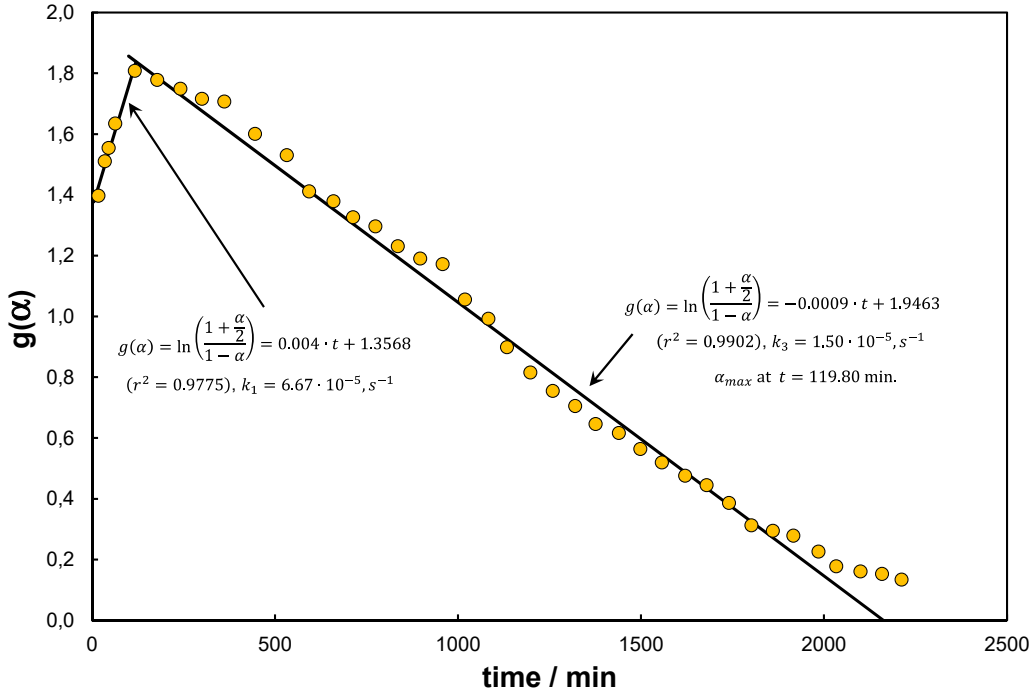

Figure 5. Experimental data for nickel catalyst; data showed in [38].

The maximum conversion degree occurs here around the 120th minute of the test, hence indicating a transition from the time scale of seconds (for the elementary reaction) to a time scale of minutes, or even hours (for the deactivation part). Equation (51) remains correct whenever takes values higher than the constant term that results for the time $t = 0$.

From the comparison of kinetic constants, it follows that when the elementary reaction is carried out under flow conditions and with the use of a catalyst, it is unnoticeable in relation to the forward reaction.

KCE and EEC

Based on the collected literature data [13,55,88,101,111,115,118–121], the parameters of the Arrhenius law were determined and then presented in a coordinate system of $(\ln A)$ vs (E) – Figure 6 (KCE). The comparison includes only the data for which the dimensions of the kinetic constant (A) could be assumed to be (s^{-1}). The pressure unit "atm" was omitted, as it can be referred to $(P°)$, while geometric dimensions were assumed for the given (or estimated) quantities. The error of this approach disappears when referring to the same conditions, while due to the use of the logarithmic value for the frequency factor its overall influence on the precision of the analysis is minimal.

 doi:10.20944/preprints202408.0065.v1

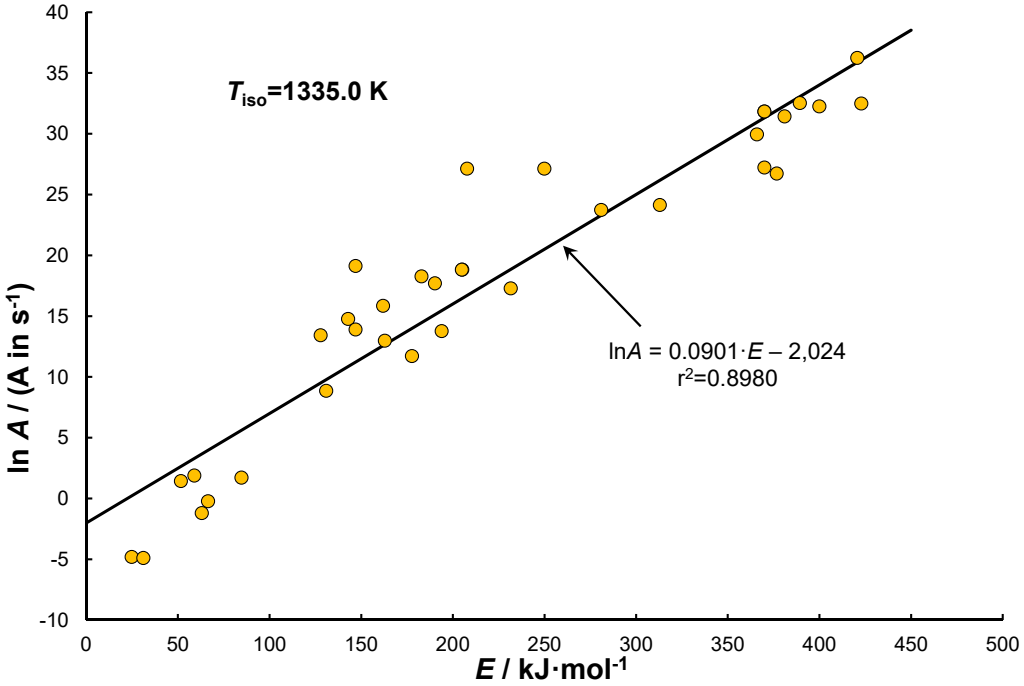

Figure 6. Parameters of Arrhenius eq. acc. to literature data in the form of KCE, $T_{iso} = 1335.0$ K

The coordinates of the chart presented in Figure 6 determine a linear relationship of KCE for the elementary reaction (1). This relationship exhibits a slight asymmetry in the range $E = 150 - 250$ kJ · mol^{-1}, which corresponds to catalysed reactions. From top the line of KCE is limited by the energy of C–H bond. Acc. to [8] its value is equal to 434 kJ · mol^{-1}, which corresponds to coordinate (420.7; 36.23). The data was obtained through experiments performed in a perfectly mixed reactor with a bypass (CPMR) [115]. As a general remark it is often understood that activation energies $E > 250$ kJ · mol^{-1} are characteristic of high-temperature pyrolysis processes initiated by the breaking of C–H bonds.

Analogously to KCE, by expressing the Arrhenius parameters using thermodynamic activation functions, it is possible to present them in the form of EEC. Figure 7 presented below depicts the EEC line for reaction (1) [62].

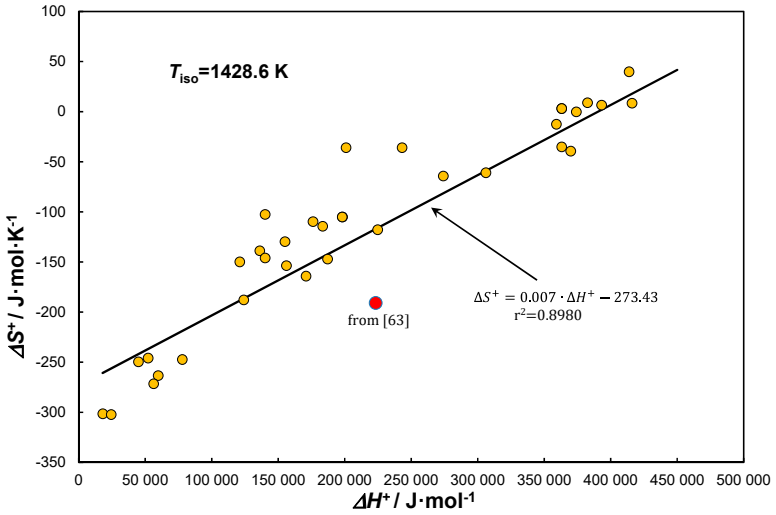

Figure 7. KCE converted to thermodynamic activation functions according to EEC. $T_{eq.} = 815.2$ K, point marked in red is outside of the range of correlation presented in Figure 6

The above expression for EEC is given in the form proposed by [95]:

 doi:10.20944/preprints202408.0065.v1

$$\Delta S^{+} = \frac{\Delta H^{+}}{T_{iso}} + \Delta S_B \tag{58}$$

where entropy of activation in isokinetic temperature ΔS_B is equal to:

$$\Delta S_B = \mathrm{R} \ln\left(\frac{k_{iso}}{\mathrm{B} T_{iso}}\right) = \mathrm{R} \ln\left(\frac{A_{E=0}}{\mathrm{B} T_{iso}}\right) \tag{59}$$

Importantly the components of Equation (58) were determined based on the following relations:

$$\Delta H^{+} = E - \mathrm{R}\, T_{eq.} \tag{60}$$

$$\Delta S^{+} = \mathrm{R}\left[\ln\left(\frac{A}{\mathrm{B} T_{eq.}}\right) - 1\right] \tag{61}$$

Eqs. (60) and (61) when introduced to Equation (58) lead to KCE with the difference that for the activation function, the equilibrium temperature $T_{eq.} = 815.2\ \mathrm{K}$ is introduced (Table 1, No 1). Reason for the above is that when T_{iso} is used here, we end up with a tautological problem; hence, here the relation to equilibrium temperature was deliberate and is proposed because both of these values are greatly different $T_{iso} > T_{eq.}$. Finally, we obtain:

$$\ln A = \frac{E}{\mathrm{R} T_{iso}} + \ln A_{E=0} + \left[1 - \frac{T_{eq.}}{T_{iso}} + \ln\left(\frac{T_{eq.}}{T_{iso}}\right)\right] \tag{62}$$

The expression in square brackets in Equation (62) equals 0 for $T_{iso} = T_{eq.}$. For example, if $T_{iso} = 2T_{eq.}$, the dimensionless sum equals approximately -0.2, and for $T_{iso} > T_{eq.}$ the calculated value adds to the intercept. Therefore, due to herein accepted reference temperatures (intercept) and the regression analysis from inversion of which T_{iso} is determined (slope), the coefficients of KCE and EEC differ.

By substituting in Equation (59) the data given in Figure 6 ($\ln k_{iso} = -2.0241$) and in Figure 7 $T_{iso} = 1428.6\ \mathrm{K}$ we obtain $\Delta S_B = -274.80 \cdot \mathrm{J} \cdot (\mathrm{mol} \cdot \mathrm{K})^{-1}$ and importantly this value is close to the intercept determined in the correlation presented on Figure 7.

Because:

$$\left(\frac{\partial \Delta_r G^{\emptyset}}{\partial T}\right)_P = -\Delta_r S^{\emptyset} \tag{63}$$

than differentiation of Eqs. (16) and (18) in regard to temperature gives that:

$$\Delta_r S^{\emptyset} = \Delta S^{+} - \Delta_{-1} S^{+} \tag{64}$$

Using Equation (61) twice on the right side of Equation (64), the term $\ln(\mathrm{B} T_{eq})$ disappears and we obtain:

$$\Delta_r S^{\emptyset} = \mathrm{R} \ln\left(\frac{A}{A_{-1}}\right) \tag{65}$$

In further considerations, we assume that T_{iso} is common for both "forwards-backwards" reactions, which is a practical approximation since we are considering two reactions occurring outside of the equilibrium temperature $T_{\mathrm{eq.}}$, for which the following $k = k_{-1}$. Based on the data from experimental study of the reaction (19), which was performed under isothermal conditions ($T = 1073 - 1313\ \mathrm{K}$) [62], for the frequency factor (A) expressed in (s^{-1}), according to Equation (65) we obtain $\Delta_r S^{\emptyset} = 100.4\ \mathrm{J} \cdot (\mathrm{mol} \cdot \mathrm{K})^{-1}$. For comparison, according to [1] for $T_{eq.} = 815.5\ \mathrm{K}$, $\Delta_r S^{\circ} = 100.5\ \mathrm{J} \cdot (\mathrm{mol} \cdot \mathrm{K})^{-1}$, while for $T = 298.15\ \mathrm{K}$, $\Delta_r S^{\circ} = 80.89\ \mathrm{J} \cdot (\mathrm{mol} \cdot \mathrm{K})^{-1}$.

The above result is consistent with expectations when compared to the slope of Equation (20). Within the range of temperatures studied in in [62], i.e. from $T_{eq.}$ to $1313\ K$ (1073–1313 K), we observe only slight variability in the increase of entropy with temperature.

Using the reference temperature $T = T_{eq.}$, one can utilize the equality $k = k_{-1}$ which implies:

 doi:10.20944/preprints202408.0065.v1

$$\ln\left(\frac{A}{A_{-1}}\right) = \frac{E - E_{-1}}{\mathrm{R}T_{eq.}} \tag{66}$$

Coupling Eqs. (65) and (66) with the condition that for $\Delta_r G^{\emptyset} = 0$ the $\Delta_r H^{\emptyset} = T_{eq.} \cdot \Delta_r S^{\emptyset}$, leads to the following simple relation:

$$\Delta_r H^{\emptyset} = E - E_{-1} \tag{67}$$

For complementarity with any given temperature, Equation (67) can be derived by combining Equation (16) with Equation (64) thus building the relationship:

$$\Delta_r H^{\emptyset} = \Delta H^{+} - \Delta_{-1} H^{+} \tag{68}$$

For the data adopted in the analysis of expression (19) [62], according to Equation (67), we obtain $\Delta_r H^{\circ} = 124.3\,\mathrm{kJ \cdot mol^{-1}}$. The same value (only with a negative sign) is given in work [62] and it is also the intercept in Equation (20). According to [1], for $T_{eq.} = 815.2\,\mathrm{K}$, $\Delta_r H^{\circ} = 87.48\,\mathrm{kJ \cdot mol^{-1}}$, and this value is close to the average enthalpy given in Table 1, No 1. The difference arises directly from the involvement of the solid phase symbolically assigned to the components $\mathrm{Fe + C/Fe_3C}$ and the inability to distinguish the composition of the solid solution of C in Fe from the cementite, thus being formed and decomposed in undefined stoichiometric ratios.

Comparing Eqs. (58) with (64) and (67) leads to the interpretation of thermal and catalytic decomposition from the perspective of activation thermodynamics and phenomenology. Equation (67) is particularly important for the reversible reaction because it fulfils the empirical observation ($E > \Delta_r H^{\circ}$).

In EEC, the intercept, which according to Equation (59) is the constant of activation entropy and assumes values < 0, occurs when the relationship $k_{\mathrm{iso}} = A_{(E=0)} < \mathrm{B}T_{\mathrm{iso}}$. According to Equation (64) the difference between activation entropy and the entropy of the initial state arises directly from the inequality $\Delta S^{+} > \Delta_{-1} S^{+}$ and because $\Delta_r S^{\circ} > 0$. Furthermore, according to Equation (67) $E > E_{-1}$.

Comparing Figs. 6 and 7 can lead to the conclusion that we are dealing with the same information. For both relationships, for $N = 35$ measurements $r^2 = 0.898$. Moreover, both are significant with a probability of 99.9%. The fundamental difference between these two lies in their interpretation. From the determined EEC line and Equation (58) the increase in activation entropy in the range $\Delta S^{+} = -200 - 100\,\mathrm{J \cdot (mol \cdot K)^{-1}}$ can be explained according to Equation (61) by the increase in reaction rate, which according to Arrhenius translates into a higher pre-exponential constant, i.e., $(\Delta S^{+} \propto \ln A)$.

This can also explain the red point below the EEC line in Figure 7 (omitted from the correlation). It can thus be debated that it indicates a significant decrease in the rate of methane decomposition under conditions of carbon absorption/dissolution by the excess solid phase $(\gamma - \mathrm{Fe})$. The conclusion is that while we use correlations expressed in terms of ratios, here Eqs. (18) and (65), the problem stands differently for absolute expressions, eg, here Eqs. (16) and (64). Expression (19) exemplifies this because the decrease in methane decomposition kinetics is related to the course of the reaction or physical process: $(3\mathrm{Fe + C} \leftrightarrow \mathrm{Fe_3C})$ (Table 1, No 5), translating only the formation of weaker bonds in the solid solution.

Considering the reaction path (19) in the reverse direction, we have no guarantee that we return to the structure symbolically written as $[\mathrm{C\ (in\ }\gamma - \mathrm{Fe})]$, because $(\gamma - \mathrm{Fe})$ cannot be a product.

The emergence of a physical transformation in the system of herein considered process, affects its kinetics in the context of the possibility for analysing its reversibility. An illustration of the Bell-Boudouard reaction (Table 1, No 12) can be Figure 1 in [122], because closing chemical cycle does not always render a return to identical structural forms.

The herein presented considerations thus strengthen the connection between the parameters of the Arrhenius law and Eyring's TST.

Discussion

 doi:10.20944/preprints202408.0065.v1

Discussion on the kinetics of methane pyrolysis reaction needs to be divided to two separate ranges of conversion degree.

Range $\alpha \rightarrow \alpha_{eq.}$

For the sake of this discussion, as a base condition Authors have adopted a technological variant of the reaction (1), where iron catalyst has the form of iron ore, and hematite serves as the reference material. The choice of such a catalyst is due to the fact that the unit price of ore is about 100 times lower than that of a nickel catalyst [57]. It should be noted though that the route from raw iron ore to an active catalytic form is rather complex. Another argument in favour of iron catalysts is the possibility of using the spent catalyst in metallurgical processes (blast furnace, foundry), which can stand as a way for decarbonization of this sector, or as a last resort the spent catalyst can be easily and safely disposed. Not only in comparison to nickel, but also within the family of different forms of iron, the primary disadvantage of iron catalysts is the need to use higher temperatures. This feature stems from lower catalytic activity and while theoretically 600–800°C is sufficient to make catalytically active $\alpha - Fe$ [49], for processes carried out in fixed bed conditions, even at 800°C the time required to conduct the process is still very long [57].

On contrary, even higher temperatures, characteristic with the polymorphic transformation of iron $t = 912°C$ (No 7 in Table 1), result in weakened catalytic activity and reduced potential for the formation of cementite (No 5 in Table 1).

Thermodynamic considerations presented in Table 1 show that when reaction (1) is performed without using a catalyst and when hematite is used, its equilibrium temperature shifts from 542°C to at least 586°C. This certainly translates into the need to increase the reaction temperature for kinetic reasons. When $t = 542°C$, $K = 1$ and from Equation (10), we get $\alpha_{eq.} = \sqrt{0.2} = 0.4472$. However, from experimentally determined data we know that at these conditions the conversion degrees will be much lower. In fact, α drops even further if we assume dilution of methane with an inert gas. For example, for $x_0 = 0.5$, from Equation (52) for $(K = 1)$ follows that $\alpha_{eq.} = 0.1708$, which in practical terms means that α is close to 0. According to Equation (57) using DFE at these temperatures narrows the scale of the adopted experimental conversion values. For $\alpha = 0$, $DFE = 1$, but for $\alpha = \alpha_{eq.} = 1$, $DFE = 0$.

These considerations indicate the possibility of adopting linear relationships of α vs time, when the reaction operates in the range of small conversion degrees. In such case Eqs. (43) and (56) find use, but this model cannot be said to adequately represent reaction (1) and thus represents only an approximation. On the other hand, the dilution of methane with an inert gas simplifies kinetic expressions. Ultimately, the increase in temperature causes the increase of conversion $\alpha_{eq.} \rightarrow 1$, which implies the possibility of ignoring the term responsible for the reversible reaction $k_{-1} = 0$.

Model F1 (No 5) presented in in Table 3 and Figure 4 indicate significant deviation of kinetic constant k_1 determined using other models. This is thought to be because the remaining models are richer in terms that more accurately describe the nature of the process involved in pyrolysis of methane. By interpreting the differential equations, it can be shown that they approach quasi-second order, which for small α is very clear for model No 2 $\left(\frac{1-\alpha}{1+\alpha} = (1-\alpha)(1+\alpha)^{-1} \cong (1-\alpha)^2\right)$.

Therefore, the basis is F1 kinetics, but modified with elements of the uncatalyzed reaction (1) during the transition from homogeneous to heterogeneous reaction. A detailed analysis of the kinetics of this type of reaction is presented in the book [110]. For flow reactors (e.g. plug flow reactor), the reaction time, measured as the residence time, is the ratio of reactor volume to flow, which results from the proportionality to the integral $\propto \int \frac{d\alpha}{r}$.

In this light, analysing the elementary reaction of the thermal process is an important element of considerations. Referring to the research results presented in Figure 3, Arrhenius parameters calculated there for $P = 5.61$ MPa, $E = 130.5\ \mathrm{kJ \cdot mol^{-1}}$, $\ln A = 8.59$ (A in $(\mathrm{s^{-1}})$), can be contrasted with results obtained for higher temperatures $> 1200°C$ and at atmospheric pressure [111–113,120], $E = 420.7\ \mathrm{kJ \cdot mol^{-1}}$, $\ln A = 36.23$ (A in $(\mathrm{s^{-1}})$). Importantly, both possibilities indicate that the reaction occurs on a second or millisecond scale.

 doi:10.20944/preprints202408.0065.v1

According to Eqs. (8) and (10) in the case of high pressure $P = 5.61\,\text{MPa}$ at $t = 900°\text{C}$, we obtain $\alpha_{eq.} = 0.4336$. Thus, the actual experimental conversion degree is less than $\alpha < 0.43$, and hence the determined characteristic Arrhenius parameters are understated.

For three types of reactors, study [115] presents a very wide range of activation energies. At the same time, [123] discusses the results of computer simulations performed for $T_{\text{iso}} = 1190.9\,\text{K}$. Importantly though in both above-mentioned works the rate constants are equal. Therefore, for all dependencies that refer to this temperature, we observe the unambiguity of the kinetic constants.

Range $\alpha \to 0$

The part of the course of methane pyrolysis, which takes place under the condition of decreasing value of conversion degree is sometimes referred to as catalyst testing. Figure 5 presented above depicts this period; however, its formal analysis boils down to calculation of the amount of carbon deposit formed, which again can be done using Eqs. (25) and (28). The results shown in Table 2 indicate that it is possible to carry out such analyses also for the range when $\alpha \to 0$. Going further, the case shown in Figure 5 confirms, the possibility of using, e.g., model No. 1 of Table 3 for methane pyrolysis reactions when $\alpha \to \alpha_{eq.}$. At the maximum (i.e. for $t^* = 119.80$ minutes) according to Eqs. (8) and (53) $\alpha_{max} = 0.7864$ while $\alpha_{eq.} = 0.8211$.

A separate issue that needs attention is whether it is possible to model the kinetics of reaction (1) in the full range of variability of its conversion degree. Till this point no such analyses were found in the literature, while some reference may be the proposals presented in [124]. The simplest form capable of describing the full range of variability of the conversion degree can be taken as an empirical formula:

$$\alpha = \frac{k_1}{k_1 - k_3}\left(e^{-k_3 t} - e^{-k_1}\right),\ k_1 > k_3 \tag{69}$$

The kinetic constants for Equation (69) are presented in this work. During the analysis of the kinetic equations, it was assumed that the basic approach describing the elementary reaction is presented in Equation (32). Further proceedings highlighted the importance of the reversible term and its impact in the case of catalysts reactive towards carbon formed during the process. In this context, it was concluded that catalysts basing their activity due to the content, availability and form of iron may be the best choice.

The paper finally presents a series of complex and extensive kinetic equations modelling individual elementary reactions responsible for the mechanism of reaction (1) with and without the use of catalyst. As a result the rate of the reaction is described by an equation generally known as the Langmuir-Hinshelwood-Hougen-Watson (LHHW) [125], with an exponent in the denominator equal to 2 (or 1), constituting the sorption term [13,109,126].

Conclusions

A literature review of the kinetics of methane thermal decomposition was conducted, focusing on finding the elementary reaction in the sense defined in the Gold Book [106], and considering the significance of the reversible term – the initial approach of Equation (32). It was found that the limitation of the efficiency of the methane thermal decomposition process is the equilibrium conversion degree and distance from equilibrium (DFE). These limitations can be mitigated by increasing the process temperature to at least 900°C and diluting methane with an inert gas, which in turn makes the reaction/process irreversible.

Detailed analyses of the non-catalytic elementary reaction of methane thermal decomposition indicate that in the case of high pressures or high temperatures and short process times (on the order of ms), the reaction kinetics can be described by the parameters of Arrhenius law. Despite the large range of activation energies $E = 130.5–420.7\,\text{kJ}\cdot\text{mol}^{-1}$, these parameters meet the Kinetic Compensation Effect (KCE) and the Enthalpy-Entropy-Compensation (EEC) for thermodynamic

 doi:10.20944/preprints202408.0065.v1

activation functions. Noteworthy in many of the catalytic processes described in literature, they occur on a much broader time scale (with long durations) extending to hours.

It has been shown that in the kinetic category of conversion degree in the presence of catalysts, the kinetic equations covering the range $\alpha \rightarrow \alpha_{max} \rightarrow \alpha_{eq.}$ can take simple forms, e.g., the F1 model. After supplementing this approach with process elements (Table 3), this model exhibits a quasi-second-order. Furthermore, conversion degree is a very convenient kinetic category, useful for balancing of the process and determining the amount of carbon deposit.

For supported catalysts based on iron, it is necessary to consider their activation. The stages of catalyst preparation, i.e., drying, grinding, sieving, and subsequent reduction of iron oxides with methane or hydrogen need to be considered. In the context of methane pyrolysis, the preferable form of iron catalyst is $\alpha - Fe$, which also constitutes the most favourable structure of Fe for the formation of cementite. Importantly the polymorphic form $\gamma - Fe$, occurring at temperatures $> 912°C$, shows lower catalytic activity. It should also be noted that the transition of iron-supported carriers to active forms of iron is a time- and reductant-consuming process.

The possibility of using the Kinetic Compensation Effect (KCE) to interpret reaction (1) and identify both synergistic and antagonistic catalytic interactions occurring in this process has been confirmed. The phenomenon becomes apparent after transforming the kinetic data according to Arrhenius into thermodynamic activation functions, i.e. Entropy-Enthalpy-Compensation (EEC). Noteworthy also Equation (58) favours activation entropy as a quantity proportional to the ratio E/T_{iso}, when $\Delta H^{+} = E - RT_{iso}$.

The thermal decomposition reaction occurring in the system containing: methane, carbon and iron at temperatures close to the isoconversion temperature depends on the proportions of components and the effects of the interactions between the Fe/C phases. Elements of the Transition State Theory (TST) were applied to the analysis of the system by comparing the ratio of "forwards-backwards" kinetic constants to the functions of phenomenological thermodynamic. Herein quantities of phenomenological thermodynamics, i.e., Gibbs free energy, enthalpy, entropy ($\Delta_r G^{\emptyset}, \Delta_r H^{\emptyset}, \Delta_r S^{\emptyset}$), were directly related with activation functions ($\Delta G^{+}, \Delta H^{+}, \Delta S^{+}$).

The analysis presented here indicates two main areas of prospective research. Firstly, it would be beneficial to enhance the description of reaction (1) by incorporating equation (69). This has not been done previously, but it permits the description of the thermal decomposition of methane in terms of the kinetic constants associated with the thermodynamic activation functions (TST). This may facilitate the integration of current knowledge regarding the course of the reaction and deactivation of catalysts. Secondly, it can be seen that further research is required on the irreversible [13], dissociative adsorption [109], and irreversible dissociative adsorption [126] models. These should be analysed in the context of reactions (2) and (3), or even described in the light of different conversion routes, such as acetylene–benzene [46].

Author Contributions: Conceptualization, A.M., T.R., and M.S.; methodology, A.M.; validation, T.R., formal analysis, M.S.; investigation, M.S.; resources, A.S.; data curation, T.R. and T.I.; writing—original draft preparation, A.M. and T.R.; writing—review and editing, T.R. and M.S.; visualization, T. R. and T.I; supervision, T.I. and A.S.; project administration, T.I.; funding acquisition, A.S. All authors have read and agreed to the published version of the manuscript.

Funding: This research received no external funding.

Data Availability Statement: The raw data supporting the conclusions of this article will be made available by the authors on request.

Conflicts of Interest: The authors declare no conflicts of interest.

Symbols

a, b constants representing mean values of enthalpy and entropy in regard to temperature, respectively kJ·mol^{-1}, kJ·(mol·K)$^{-1}$, Table 1;

A pre-exponential factor, s^{-1};

 doi:10.20944/preprints202408.0065.v1

B 2.08364·10[10] $K^{-1}\cdot s^{-1}$, ratio of Boltzmann to Planck's constant;
c auxiliary quantity in Equation (48);
c_P heat capacities, $J\cdot(kg\cdot K)^{-1}$;
$[C]$ calculated ration of carbon deposit, $g\cdot g_{cat}^{-1}$;
E activation energy, $J\cdot mol^{-1}$;
$g(x), g(\alpha), g(z)$
kinetic functions ($g(\dots) = k_1 \cdot t$) for methane, conversion degree and thermodynamic efficiency respectively;
$\Delta G, \Delta H, \Delta S$
thermodynamic functions for free enthalpy, enthalpy and entropy respectively;
k kinetic rate constant, dependent on T, s^{-1},
K equilibrium constant,
n exponent,
P pressure or partial pressure, Pa,
r reaction rate, Eqs. (30) and (33), s^{-1};
$r(t)$ reaction rate, Equation (29), $mmol\cdot(g_{cat}\cdot time)^{-1}$;
r_0 initial reaction rate, $mmol\cdot(g_{cat}\cdot time)^{-1}$, $r_0 = const$, Equation (29);
r_C initial reaction rate, $mmol\cdot(g_{cat}\cdot time)^{-1}$, Equation (26);
r^2 linear determination coefficient, $0 \leq r^2 \leq 1$;
R R=8.314 $J\cdot(mol\cdot K)^{-1}$ universal gas constant;
$t$time, s, min and hrs;
$t$temperature, °C; (only in text)
T absolute temperature, K;
$\dot{V}$ flow rate, dm^3 or $m^3\cdot(g_{cat}\cdot time)^{-1}$;
x mol fraction, $0 \leq x \leq 1$;
z thermodynamic efficiency, $0 \leq z \leq 1$;
α conversion degree, $0 \leq \alpha \leq 1$;
β physical dilatation factor, acc. [111], Table 3;
ε expansion factor, fractional volume change on complete, conversion of substance A, acc. to [110], Table 3;
τ_D time constant for deactivation, s;
ν stoichiometric coefficient;

Subscripts

B activation entropy in isokinetic temperature;
CH_4, H_2 acc. to methane, hydrogen,
iso isokinetic,
$eq.$ equilibrium,
P pressure,
x, α acc. to equilibrium constant,
0 initial state,
1, -1, 3 acc. to: forwards, backwards and another kind,

Superscripts

$+$ activation functions;
$\emptyset$ standard state;
*maximum;
¯average;

 doi:10.20944/preprints202408.0065.v1

Abbreviations

BCC	body-centred cubic,
CPMR	Perfectly mixed reactor with bypass (in [117]),
DFE	Distance From Equilibrium (or far from equilibrium),
EEC	Enthalpy-Entropy-Compensation or (rarely) Entropy-Enthalpy-Compensation (e.g. [127]),
FCC	face-centred cubic,
KCE	Kinetic Compensation Effect,
LHHW	Langmuir-Hinshelwood-Hougen-Watson Equation,
R-WGS	Reverse Water-Gas Shift reaction,
TST	Transition-State Theory,
WGS	Water-Gas Shift reaction,
WHSV	Weight Hourly Space Velocity.

Reference

1. Barin, I. *Thermochemical Data of Pure Substances*; 1st ed.; Wiley, 1995; ISBN 978-3-527-28745-1.
2. Fierro, J.L.G. Catalysis in C1 Chemistry: Future and Prospect. *Catal Lett* **1993**, *22*, 67–91, doi:10.1007/BF00811770.
3. Msheik, M.; Rodat, S.; Abanades, S. Experimental Comparison of Solar Methane Pyrolysis in Gas-Phase and Molten-Tin Bubbling Tubular Reactors. *Energy* **2022**, *260*, 124943, doi:10.1016/j.energy.2022.124943.
4. Sánchez-Bastardo, N.; Schlögl, R.; Ruland, H. Methane Pyrolysis for Zero-Emission Hydrogen Production: A Potential Bridge Technology from Fossil Fuels to a Renewable and Sustainable Hydrogen Economy. *Ind. Eng. Chem. Res.* **2021**, *60*, 11855–11881, doi:10.1021/acs.iecr.1c01679.
5. Sánchez-Bastardo, N.; Schlögl, R.; Ruland, H. Methane Pyrolysis for CO2 -Free H2 Production: A Green Process to Overcome Renewable Energies Unsteadiness. *Chemie Ingenieur Technik* **2020**, *92*, 1596–1609, doi:10.1002/cite.202000029.
6. Xu, R.; Meisner, J.; Chang, A.M.; Thompson, K.C.; Martínez, T.J. First Principles Reaction Discovery: From the Schrodinger Equation to Experimental Prediction for Methane Pyrolysis. *Chem. Sci.* **2023**, *14*, 7447–7464, doi:10.1039/D3SC01202F.
7. Ashik, U.P.M.; Wan Daud, W.M.A.; Abbas, H.F. Production of Greenhouse Gas Free Hydrogen by Thermocatalytic Decomposition of Methane – A Review. *Renewable and Sustainable Energy Reviews* **2015**, *44*, 221–256, doi:10.1016/j.rser.2014.12.025.
8. Hamdani, I.R.; Ahmad, A.; Chulliyil, H.M.; Srinivasakannan, C.; Shoaibi, A.A.; Hossain, M.M. Thermocatalytic Decomposition of Methane: A Review on Carbon-Based Catalysts. *ACS Omega* **2023**, *8*, 28945–28967, doi:10.1021/acsomega.3c01936.
9. Audier, M.; Coulon, M.; Bonnetain, L. Hydrogenation of Catalytic Carbons Obtained by CO Disproportionation or CH4 Decomposition on Nickel. *Carbon* **1979**, *17*, 391–394, doi:10.1016/0008-6223(79)90052-6.
10. Rostrupnielsen, J. Sulfur-Passivated Nickel Catalysts for Carbon-Free Steam Reforming of Methane. *Journal of Catalysis* **1984**, *85*, 31–43, doi:10.1016/0021-9517(84)90107-6.
11. Bernardo, C.A.; Rostrup-Nielsen, J.R. Carbon Deposition and Methane Steam Reforming on Silica-Supported Ni-Cu Catalysts. *Journal of Catalysis* **1985**, *96*, 517–534, doi:https://doi.org/10.1016/0021-9517(85)90320-3.
12. Alstrup, I.; Tavares, M.T. Kinetics of Carbon Formation from CH4 + H2 on Silica-Supported Nickel and Ni-Cu Catalysts. *Journal of Catalysis* **1993**, *139*, 513–524, doi:10.1006/jcat.1993.1045.
13. Snoeck, J.-W.; Froment, G.F.; Fowles, M. Kinetic Study of the Carbon Filament Formation by Methane Cracking on a Nickel Catalyst. *Journal of Catalysis* **1997**, *169*, 250–262, doi:10.1006/jcat.1997.1635.
14. Kuvshinov, G.G.; Mogilnykh, Yu.I.; Kuvshinov, D.G. Kinetics of Carbon Formation from CH4–H2 Mixtures over a Nickel Containing Catalyst. *Catalysis Today* **1998**, *42*, 357–360, doi:10.1016/S0920-5861(98)00115-1.
15. Chambers, A.; Nemes, T.; Rodriguez, N.M.; Baker, R.T.K. Catalytic Behavior of Graphite Nanofiber Supported Nickel Particles. 1. Comparison with Other Support Media. *J. Phys. Chem. B* **1998**, *102*, 2251–2258, doi:10.1021/jp973462g.
16. Li, Y.; Chen, J.; Qin, Y.; Chang, L. Simultaneous Production of Hydrogen and Nanocarbon from Decomposition of Methane on a Nickel-Based Catalyst. *Energy Fuels* **2000**, *14*, 1188–1194, doi:10.1021/ef0000781.
17. Ermakova, M.A.; Ermakov, D.Y.; Kuvshinov, G.G. Effective Catalysts for Direct Cracking of Methane to Produce Hydrogen and FIlamentous Carbon Part I. Nickel Catalysts. **2000**.

18. Otsuka, K.; Ogihara, H.; Takenaka, S. Decomposition of Methane over Ni Catalysts Supported on Carbon Fibers Formed from Different Hydrocarbons. *Carbon* **2003**, *41*, 223–233, doi:10.1016/S0008-6223(02)00308-1.
19. Qian, W.; Liu, T.; Wei, F.; Wang, Z.; Li, Y. Enhanced Production of Carbon Nanotubes: Combination of Catalyst Reduction and Methane Decomposition. *Applied Catalysis A: General* **2004**, *258*, 121–124, doi:10.1016/j.apcata.2003.08.017.
20. Villacampa, J.I.; Royo, C.; Romeo, E.; Montoya, J.A.; Del Angel, P.; Monzón, A. Catalytic Decomposition of Methane over Ni-Al2O3 Coprecipitated Catalysts. *Applied Catalysis A: General* **2003**, *252*, 363–383, doi:10.1016/S0926-860X(03)00492-7.
21. Otsuka, K.; Takenaka, S.; Ohtsuki, H. Production of Pure Hydrogen by Cyclic Decomposition of Methane and Oxidative Elimination of Carbon Nanofibers on Supported-Ni-Based Catalysts. *Applied Catalysis A: General* **2004**, *273*, 113–124, doi:10.1016/j.apcata.2004.06.021.
22. Sharif Zein, S.H.; Mohamed, A.R.; Talpa Sai, P.S. Kinetic Studies on Catalytic Decomposition of Methane to Hydrogen and Carbon over Ni/TiO 2 Catalyst. *Ind. Eng. Chem. Res.* **2004**, *43*, 4864–4870, doi:10.1021/ie034208f.
23. Dupuis, A. The Catalyst in the CCVD of Carbon Nanotubes—a Review. *Progress in Materials Science* **2005**, *50*, 929–961, doi:10.1016/j.pmatsci.2005.04.003.
24. Chen, D.; Christensen, K.; Ochoafernandez, E.; Yu, Z.; Totdal, B.; Latorre, N.; Monzon, A.; Holmen, A. Synthesis of Carbon Nanofibers: Effects of Ni Crystal Size during Methane Decomposition. *Journal of Catalysis* **2005**, *229*, 82–96, doi:10.1016/j.jcat.2004.10.017.
25. Venugopal, A.; Naveen Kumar, S.; Ashok, J.; Hari Prasad, D.; Durga Kumari, V.; Prasad, K.B.S.; Subrahmanyam, M. Hydrogen Production by Catalytic Decomposition of Methane over Ni/SiO2Ni/SiO2☆. *International Journal of Hydrogen Energy* **2007**, *32*, 1782–1788, doi:10.1016/j.ijhydene.2007.01.007.
26. Bai, Z.; Chen, H.; Li, B.; Li, W. Methane Decomposition over Ni Loaded Activated Carbon for Hydrogen Production and the Formation of Filamentous Carbon. *International Journal of Hydrogen Energy* **2007**, *32*, 32–37, doi:10.1016/j.ijhydene.2006.06.030.
27. Pinilla, J.L.; Suelves, I.; Lázaro, M.J.; Moliner, R.; Palacios, J.M. Parametric Study of the Decomposition of Methane Using a NiCu/Al2O3 Catalyst in a Fluidized Bed Reactor. *International Journal of Hydrogen Energy* **2010**, *35*, 9801–9809, doi:10.1016/j.ijhydene.2009.10.008.
28. De Jesús, J.C.; González, I.; García, M.; Urbina, C. Preparation of Nickel Nanoparticles and Their Catalytic Activity in the Cracking of Methane. *Journal of Vacuum Science & Technology A: Vacuum, Surfaces, and Films* **2008**, *26*, 913–918, doi:10.1116/1.2885212.
29. Suelves, I.; Pinilla, J.L.; Lázaro, M.J.; Moliner, R.; Palacios, J.M. Effects of Reaction Conditions on Hydrogen Production and Carbon Nanofiber Properties Generated by Methane Decomposition in a Fixed Bed Reactor Using a NiCuAl Catalyst. *Journal of Power Sources* **2009**, *192*, 35–42, doi:10.1016/j.jpowsour.2008.11.096.
30. Cunha, A.F.; Órfão, J.J.M.; Figueiredo, J.L. Methane Decomposition on Ni–Cu Alloyed Raney-Type Catalysts. *International Journal of Hydrogen Energy* **2009**, *34*, 4763–4772, doi:10.1016/j.ijhydene.2009.03.040.
31. Chesnokov, V.V.; Chichkan, A.S. Production of Hydrogen by Methane Catalytic Decomposition over Ni–Cu–Fe/Al2O3 Catalyst. *International Journal of Hydrogen Energy* **2009**, *34*, 2979–2985, doi:10.1016/j.ijhydene.2009.01.074.
32. Salmones, J.; Wang, J.A.; Valenzuela, M.A.; Sánchez, E.; Garcia, A. Pore Geometry Influence on the Deactivation Behavior of Ni-Based Catalysts for Simultaneous Production of Hydrogen and Nanocarbon. *Catalysis Today* **2009**, *148*, 134–139, doi:10.1016/j.cattod.2009.03.005.
33. Zapata, B.; Valenzuela, M.A.; Palacios, J.; Torres-Garcia, E. Effect of Ca, Ce or K Oxide Addition on the Activity of Ni/SiO2 Catalysts for the Methane Decomposition Reaction. *International Journal of Hydrogen Energy* **2010**, *35*, 12091–12097, doi:10.1016/j.ijhydene.2009.09.072.
34. Hussain, T.; Iqbal, M. Pyrolysis of Methane by Catalytic Properties Exhibited by Ceramics. *Journal of Analytical and Applied Pyrolysis* **2011**, *90*, 106–111, doi:10.1016/j.jaap.2010.10.012.
35. Saraswat, S.K.; Pant, K.K. Ni–Cu–Zn/MCM-22 Catalysts for Simultaneous Production of Hydrogen and Multiwall Carbon Nanotubes via Thermo-Catalytic Decomposition of Methane. *International Journal of Hydrogen Energy* **2011**, *36*, 13352–13360, doi:10.1016/j.ijhydene.2011.07.102.
36. Nuernberg, G.D.B.; Foletto, E.L.; Campos, C.E.M.; Fajardo, H.V.; Carreño, N.L.V.; Probst, L.F.D. Direct Decomposition of Methane over Ni Catalyst Supported in Magnesium Aluminate. *Journal of Power Sources* **2012**, *208*, 409–414, doi:10.1016/j.jpowsour.2012.02.037.
37. Hornés, A.; Bera, P.; Fernández-García, M.; Guerrero-Ruiz, A.; Martínez-Arias, A. Catalytic and Redox Properties of Bimetallic Cu–Ni Systems Combined with CeO2 or Gd-Doped CeO2 for Methane Oxidation and Decomposition. *Applied Catalysis B: Environmental* **2012**, *111–112*, 96–105, doi:10.1016/j.apcatb.2011.09.022.
38. Saraswat, S.K.; Pant, K.K. Synthesis of Hydrogen and Carbon Nanotubes over Copper Promoted Ni/SiO2 Catalyst by Thermocatalytic Decomposition of Methane. *Journal of Natural Gas Science and Engineering* **2013**, *13*, 52–59, doi:10.1016/j.jngse.2013.04.001.

39. Wang, H.Y.; Lua, A.C. Deactivation and Kinetic Studies of Unsupported Ni and Ni–Co–Cu Alloy Catalysts Used for Hydrogen Production by Methane Decomposition. *Chemical Engineering Journal* **2014**, *243*, 79–91, doi:10.1016/j.cej.2013.12.100.
40. Tang, M.; Xu, L.; Fan, M. Progress in Oxygen Carrier Development of Methane-Based Chemical-Looping Reforming: A Review. *Applied Energy* **2015**, *151*, 143–156, doi:10.1016/j.apenergy.2015.04.017.
41. Ashik, U.P.M.; Wan Daud, W.M.A.; Abbas, H.F. Methane Decomposition Kinetics and Reaction Rate over Ni/SiO2 Nanocatalyst Produced through Co-Precipitation Cum Modified Stöber Method. *International Journal of Hydrogen Energy* **2017**, *42*, 938–952, doi:10.1016/j.ijhydene.2016.09.025.
42. Keipi, T.; Tolvanen, K.E.S.; Tolvanen, H.; Konttinen, J. Thermo-Catalytic Decomposition of Methane: The Effect of Reaction Parameters on Process Design and the Utilization Possibilities of the Produced Carbon. *Energy Conversion and Management* **2016**, *126*, 923–934, doi:10.1016/j.enconman.2016.08.060.
43. Łamacz, A. CNT and H2 Production During CH4 Decomposition over Ni/CeZrO2. I. A Mechanistic Study. *ChemEngineering* **2019**, *3*, 26, doi:10.3390/chemengineering3010026.
44. Łamacz, A.; Łabojko, G. CNT and H2 Production during CH4 Decomposition over Ni/CeZrO2. II. Catalyst Performance and Its Regeneration in a Fluidized Bed. *ChemEngineering* **2019**, *3*, 25, doi:10.3390/chemengineering3010025.
45. Muto, T.; Asahara, M.; Miyasaka, T.; Asato, K.; Uehara, T.; Koshi, M. Methane Pyrolysis Characteristics for the Practical Application of Hydrogen Production System Using Permalloy Plate Catalyst. *Chemical Engineering Science* **2023**, *274*, 117931, doi:10.1016/j.ces.2022.117931.
46. Park, S.; Kim, M.; Koo, Y.; Kang, D.; Kim, Y.; Park, J.; Ryu, C. Numerical Modeling of Methane Pyrolysis in a Bubble Column of Molten Catalysts for Clean Hydrogen Production. *International Journal of Hydrogen Energy* **2023**, *48*, 7385–7399, doi:10.1016/j.ijhydene.2022.11.068.
47. Harrath, K.; Yao, Z.; Jiang, Y.-F.; Wang, Y.-G.; Li, J. Activity Origin of the Nickel Cluster on TiC Support for Nonoxidative Methane Conversion. *J. Phys. Chem. Lett.* **2023**, *14*, 4033–4041, doi:10.1021/acs.jpclett.3c00375.
48. Yan, P.; Zhang, K.; Peng, Y. Study of Fe2O3-Al2O3 Catalyst Reduction Parameters and Conditions for Catalytic Methane Decomposition. *Chemical Engineering Science* **2022**, *250*, 117410, doi:10.1016/j.ces.2021.117410.
49. Ermakova, M.A.; Ermakov, D.Y.; Chuvilin, A.L.; Kuvshinov, G.G. Decomposition of Methane over Iron Catalysts at the Range of Moderate Temperatures: The Influence of Structure of the Catalytic Systems and the Reaction Conditions on the Yield of Carbon and Morphology of Carbon Filaments. *Journal of Catalysis* **2001**, *201*, 183–197, doi:10.1006/jcat.2001.3243.
50. Ermakova, M. Ni/SiO2 and Fe/SiO2 Catalysts for Production of Hydrogen and Filamentous Carbon via Methane Decomposition. *Catalysis Today* **2002**, *77*, 225–235, doi:10.1016/S0920-5861(02)00248-1.
51. Reshetenko, T. Coprecipitated Iron-Containing Catalysts (Fe-Al2O3, Fe-Co-Al2O3, Fe-Ni-Al2O3) for Methane Decomposition at Moderate temperaturesI. Genesis of Calcined and Reduced Catalysts. *Applied Catalysis A: General* **2004**, *268*, 127–138, doi:10.1016/j.apcata.2004.03.045.
52. Konieczny, A.; Mondal, K.; Wiltowski, T.; Dydo, P. Catalyst Development for Thermocatalytic Decomposition of Methane to Hydrogen. *International Journal of Hydrogen Energy* **2008**, *33*, 264–272, doi:10.1016/j.ijhydene.2007.07.054.
53. Balakrishnan, M.; Batra, V.S.; Hargreaves, J.S.J.; Monaghan, A.; Pulford, I.D.; Rico, J.L.; Sushil, S. Hydrogen Production from Methane in the Presence of Red Mud –Making Mud Magnetic. *Green Chem.* **2009**, *11*, 42–47, doi:10.1039/B815834G.
54. Pinilla, J.L.; Utrilla, R.; Karn, R.K.; Suelves, I.; Lázaro, M.J.; Moliner, R.; García, A.B.; Rouzaud, J.N. High Temperature Iron-Based Catalysts for Hydrogen and Nanostructured Carbon Production by Methane Decomposition. *International Journal of Hydrogen Energy* **2011**, *36*, 7832–7843, doi:10.1016/j.ijhydene.2011.01.184.
55. Kashiwaya, Y.; Watanabe, M. Kinetic Analysis of the Decomposition Reaction of CH4 Injecting into Molten Slag. *ISIJ Int.* **2012**, *52*, 1394–1403, doi:10.2355/isijinternational.52.1394.
56. Torres, D.; De Llobet, S.; Pinilla, J.L.; Lázaro, M.J.; Suelves, I.; Moliner, R. Hydrogen Production by Catalytic Decomposition of Methane Using a Fe-Based Catalyst in a Fluidized Bed Reactor. *Journal of Natural Gas Chemistry* **2012**, *21*, 367–373, doi:10.1016/S1003-9953(11)60378-2.
57. Cornejo, A. The Thermo-Catalytic Decomposition of Methane for Economical and Emission-Free Hydrogen Production; 2013;
58. Alves Silva, J.; Oliveira Santos, J.B.; Torres, D.; Pinilla, J.L.; Suelves, I. Natural Fe-Based Catalysts for the Production of Hydrogen and Carbon Nanomaterials via Methane Decomposition. *International Journal of Hydrogen Energy* **2021**, *46*, 35137–35148, doi:10.1016/j.ijhydene.2021.08.065.
59. Lumbers, B.; Barley, J.; Platte, F. Low-Emission Hydrogen Production via the Thermo-Catalytic Decomposition of Methane for the Decarbonisation of Iron Ore Mines in Western Australia. *International Journal of Hydrogen Energy* **2022**, *47*, 16347–16361, doi:10.1016/j.ijhydene.2022.03.124.

60. Vlaskin, M.S.; Grigorenko, A.V.; Gromov, A.A.; Kumar, V.; Dudoladov, A.O.; Slavkina, O.V.; Darishchev, V.I. Methane Pyrolysis on Sponge Iron Powder for Sustainable Hydrogen Production. *Results in Engineering* **2022**, *15*, 100598, doi:10.1016/j.rineng.2022.100598.
61. Wojtasik, M. Dekarbonizacja Metanu z Udziałem Katalizatorów Na Bazie Żelaza. *CHEMICAL REVIEW* **2023**, *1*, 55–59, doi:10.15199/62.2023.3.4.
62. Grabke, H. -J. Die Kinetik der Entkohlung und Aufkohlung von γ-Eisen in Methan-Wasserstoff-Gemischen. *Ber Bunsenges Phys Chem* **1965**, *69*, 409–414, doi:10.1002/bbpc.19650690508.
63. Zhang, J.; Ostrovski, O. Cementite Formation in CH4-H2-Ar Gas Mixture and Cementite Stability. *ISIJ International* **2001**, *41*, 333–339, doi:10.2355/isijinternational.41.333.
64. А.н, М.; А.м, Г. Термодинамические Функции Реакций Восстановления Титаномагнетитового Концентрата Аджинаурских Песчаников Природным Газом. *Azerbaijan Chemical Journal* **2016**, 99–102.
65. Zhou, L.; Enakonda, L.R.; Harb, M.; Saih, Y.; Aguilar-Tapia, A.; Ould-Chikh, S.; Hazemann, J.; Li, J.; Wei, N.; Gary, D.; et al. Fe Catalysts for Methane Decomposition to Produce Hydrogen and Carbon Nano Materials. *Applied Catalysis B: Environmental* **2017**, *208*, 44–59, doi:10.1016/j.apcatb.2017.02.052.
66. Wang, I.-W.; Kutteri, D.A.; Gao, B.; Tian, H.; Hu, J. Methane Pyrolysis for Carbon Nanotubes and CO_x -Free H_2 over Transition-Metal Catalysts. *Energy Fuels* **2019**, *33*, 197–205, doi:10.1021/acs.energyfuels.8b03502.
67. Chuayboon, S.; Abanades, S.; Rodat, S. Stepwise Solar Methane Reforming and Water-Splitting via Lattice Oxygen Transfer in Iron and Cerium Oxides. *Energy Tech* **2020**, *8*, 1900415, doi:10.1002/ente.201900415.
68. Schneider, A.; Inden, G. Carbon Diffusion in Cementite (Fe3C) and Hägg Carbide (Fe5C2). *Calphad* **2007**, *31*, 141–147, doi:10.1016/j.calphad.2006.07.008.
69. Nikolussi, M.; Leineweber, A.; Mittemeijer, E.J. Growth of Massive Cementite Layers; Thermodynamic Parameters and Kinetics. *J Mater Sci* **2009**, *44*, 770–777, doi:10.1007/s10853-008-3160-6.
70. Hallstedt, B.; Djurovic, D.; Von Appen, J.; Dronskowski, R.; Dick, A.; Körmann, F.; Hickel, T.; Neugebauer, J. Thermodynamic Properties of Cementite (). *Calphad* **2010**, *34*, 129–133, doi:10.1016/j.calphad.2010.01.004.
71. Litasov, K.D.; Sharygin, I.S.; Dorogokupets, P.I.; Shatskiy, A.; Gavryushkin, P.N.; Sokolova, T.S.; Ohtani, E.; Li, J.; Funakoshi, K. Thermal Equation of State and Thermodynamic Properties of Iron Carbide Fe_3C to 31 GPa and 1473 K. *JGR Solid Earth* **2013**, *118*, 5274–5284, doi:10.1002/2013JB010270.
72. Vogric, M.; Kozeschnik, E.; Svoboda, J.; Führer, M.; Kreyca, J.; Wei, W.; Povoden-Karadeniz, E. Kinetic Modeling of Grain Boundary Cementite Evolution. *Metall Mater Trans A* **2022**, *53*, 3759–3773, doi:10.1007/s11661-022-06784-1.
73. Wu, M.; Li, Z.; Huang, J.; Wang, Q.; Li, T.; Yang, S.; He, H.; Jiang, Y. Non-Isothermal Kinetics of Coke and Iron Ore Melting Reduction with Variable Activation Energy Model. *Fuel* **2024**, *357*, 129991, doi:10.1016/j.fuel.2023.129991.
74. Holmen, A.; Olsvik, O.; Rokstad, O.A. Pyrolysis of Natural Gas: Chemistry and Process Concepts. *Fuel Processing Technology* **1995**, *42*, 249–267, doi:10.1016/0378-3820(94)00109-7.
75. Sinaki, M.Y.; Matida, E.A.; Hamdullahpur, F. Development of a Reaction Mechanism for Predicting Hydrogen Production from Homogeneous Decomposition of Methane. *International Journal of Hydrogen Energy* **2011**, *36*, 2936–2944, doi:10.1016/j.ijhydene.2010.12.002.
76. Boretti, A. A Perspective on the Production of Hydrogen from Solar-Driven Thermal Decomposition of Methane. *International Journal of Hydrogen Energy* **2021**, *46*, 34509–34514, doi:10.1016/j.ijhydene.2021.07.234.
77. Kim, S.E.; Jeong, S.K.; Park, K.T.; Lee, K.-Y.; Kim, H.J. Effect of Oxygen-Containing Functional Groups in Metal-Free Carbon Catalysts on the Decomposition of Methane. *Catalysis Communications* **2021**, *148*, 106167, doi:10.1016/j.catcom.2020.106167.
78. Lott, P.; Mokashi, M.B.; Müller, H.; Heitlinger, D.J.; Lichtenberg, S.; Shirsath, A.B.; Janzer, C.; Tischer, S.; Maier, L.; Deutschmann, O. Hydrogen Production and Carbon Capture by Gas-Phase Methane Pyrolysis: A Feasibility Study. *ChemSusChem* **2023**, *16*, e202201720, doi:10.1002/cssc.202201720.
79. Bae, D.; Kim, Y.; Ko, E.H.; Ju Han, S.; Lee, J.W.; Kim, M.; Kang, D. Methane Pyrolysis and Carbon Formation Mechanisms in Molten Manganese Chloride Mixtures. *Applied Energy* **2023**, *336*, 120810, doi:10.1016/j.apenergy.2023.120810.
80. Miri, S.S.; Meshkani, F.; Rastegarpanah, A.; Rezaei, M. Influence of Fe, La, Zr, Ce, and Ca on the Catalytic Performance and Coke Formation in Dry Reforming of Methane over Ni/MgO.Al2O3 Catalyst. *Chemical Engineering Science* **2022**, *250*, 116956, doi:10.1016/j.ces.2021.116956.
81. Guéret, C.; Daroux, M.; Billaud, F. Methane Pyrolysis: Thermodynamics. *Chemical Engineering Science* **1997**, *52*, 815–827, doi:10.1016/S0009-2509(96)00444-7.
82. Steinberg, M. Production of Hydrogen and Methanol from Natural Gas with Reduced CO2 Emission. *International Journal of Hydrogen Energy* **1998**, *23*, 419–425, doi:10.1016/S0360-3199(97)00092-X.
83. Zavarukhin, S.G.; Kuvshinov, G.G. The Kinetic Model of Formation of Nanofibrous Carbon from CH4–H2 Mixture over a High-Loaded Nickel Catalyst with Consideration for the Catalyst Deactivation. *Applied Catalysis A: General* **2004**, *272*, 219–227, doi:10.1016/j.apcata.2004.05.044.

84. Hofberger, C.M.; Dietrich, B.; Durán Vera, I.; Krumholz, R.; Stoppel, L.; Uhlenbruck, N.; Wetzel, T. Natural Gas Pyrolysis in a Liquid Metal Bubble Column Reaction System—Part I: Experimental Setup and Methods. *Hydrogen* **2023**, *4*, 295–306, doi:10.3390/hydrogen4020021.
85. Chase, M.W. NIST-JANAF Themochemical Tables, Fourth Edition.
86. Hossain, M.M.; De Lasa, H.I. Chemical-Looping Combustion (CLC) for Inherent CO 2 Separations—a Review. *Chemical Engineering Science* **2008**, *63*, 4433–4451, doi:10.1016/j.ces.2008.05.028.
87. Monazam, E.R.; Breault, R.W.; Siriwardane, R.; Richards, G.; Carpenter, S. Kinetics of the Reduction of Hematite (Fe2O3) by Methane (CH4) during Chemical Looping Combustion: A Global Mechanism. *Chemical Engineering Journal* **2013**, *232*, 478–487, doi:10.1016/j.cej.2013.07.091.
88. Keller, M.; Matsumura, A.; Sharma, A. Spray-Dried Fe/Al2O3 as a Carbon Carrier for COx-Free Hydrogen Production via Methane Cracking in a Fluidized Bed Process. *Chemical Engineering Journal* **2020**, *398*, 125612, doi:10.1016/j.cej.2020.125612.
89. Bagdavadze, J.; Kandelaki, A.; Ukleba, K.; Tsikaridze, Z. Thermodynamic Analysis of CoO, NiO, CuO, FeO Interaction with Methane. *BULLETIN OF THE GEORGIAN NATIONAL ACADEMY OF SCIENCES* **2021**, *4*.
90. Koytsoumpa, E.I.; Karellas, S. Equilibrium and Kinetic Aspects for Catalytic Methanation Focusing on CO2 Derived Substitute Natural Gas (SNG). *Renewable and Sustainable Energy Reviews* **2018**, *94*, 536–550, doi:10.1016/j.rser.2018.06.051.
91. SALA, C. Study of Reverse Water Gas Shift Reaction Using Bimetallic Catalysts on Active Supports 2022.
92. Vannier, D. Kinetic Study of High Temperature Water Gas Shift Reaction.
93. Frick, V.; Brellochs, J.; Specht, M. Application of Ternary Diagrams in the Design of Methanation Systems. *Fuel Processing Technology* **2014**, *118*, 156–160, doi:10.1016/j.fuproc.2013.08.022.
94. Mianowski, A.; Robak, Z.; Tomaszewicz, M.; Stelmach, S. The Boudouard–Bell Reaction Analysis under High Pressure Conditions. *J Therm Anal Calorim* **2012**, *110*, 93–102, doi:10.1007/s10973-012-2334-2.
95. Mianowski, A.; Radko, T.; Bigda, R. Elements of Transition-State Theory in Relation to the Thermal Dissociation of Selected Solid Compounds. *Energies* **2024**, *17*, 2669, doi:10.3390/en17112669.
96. Eyring, H. The Activated Complex in Chemical Reactions. *The Journal of Chemical Physics* **1935**, *3*, 107–115, doi:10.1063/1.1749604.
97. Laidler, K.J.; King, M.C. Development of Transition-State Theory. *J. Phys. Chem.* **1983**, *87*, 2657–2664, doi:10.1021/j100238a002.
98. Chi, J.W.H.; Landahl, C.E. Hydrogen Reactions with Graphite Materials at High Temperatures and Pressures. *Nuclear Applications* **1968**, *4*, 159–169, doi:10.13182/NT68-A26380.
99. Riley, J.; Atallah, C.; Siriwardane, R.; Stevens, R. Technoeconomic Analysis for Hydrogen and Carbon Co-Production via Catalytic Pyrolysis of Methane. *International Journal of Hydrogen Energy* **2021**, *46*, 20338–20358, doi:10.1016/j.ijhydene.2021.03.151.
100. Abbas, H.F.; Baker, I.F. Thermocatalytic Decomposition of Methane Using Activated Carbon: Studying the Influence of Process Parameters Using Factorial Design. *International Journal of Hydrogen Energy* **2011**, *36*, 8985–8993, doi:10.1016/j.ijhydene.2011.05.005.
101. Lee, E.K.; Lee, S.Y.; Han, G.Y.; Lee, B.K.; Lee, T.-J.; Jun, J.H.; Yoon, K.J. Catalytic Decomposition of Methane over Carbon Blacks for CO2-Free Hydrogen Production. *Carbon* **2004**, *42*, 2641–2648, doi:10.1016/j.carbon.2004.06.003.
102. Muradov, N.; Smith, F.; T-Raissi, A. Catalytic Activity of Carbons for Methane Decomposition Reaction. *Catalysis Today* **2005**, *102–103*, 225–233, doi:10.1016/j.cattod.2005.02.018.
103. Kim, M. Hydrogen Production by Catalytic Decomposition of Methane over Activated Carbons: Kinetic Study. *International Journal of Hydrogen Energy* **2004**, *29*, 187–193, doi:10.1016/S0360-3199(03)00111-3.
104. Becker, T.; Richter, M.; Agar, D.W. Methane Pyrolysis: Kinetic Studies and Mechanical Removal of Carbon Deposits in Reactors of Different Materials. *International Journal of Hydrogen Energy* **2023**, *48*, 2112–2129, doi:10.1016/j.ijhydene.2022.10.069.
105. Abanades, S.; Flamant, G. Experimental Study and Modeling of a High-Temperature Solar Chemical Reactor for Hydrogen Production from Methane Cracking. *International Journal of Hydrogen Energy* **2007**, *32*, 1508–1515, doi:10.1016/j.ijhydene.2006.10.038.
106. Chemistry (IUPAC), T.I.U. of P. and A. IUPAC - Elementary Reaction (E02035) Available online: https://goldbook.iupac.org/terms/view/E02035 (accessed on 9 July 2024).
107. Kobayashi, A.; Steinberg, M. *The Thermal Decomposition of Methane in a Tubular Reactor*; Brookhaven National Lab. (BNL), Upton, NY (United States), 1992;
108. Dahme, A.; Junker, H.J. Die Reaktivität von Koks gegen CO2 im temperaturbereich 1000–1200oC. *Brennst. Chem. 36*, 193–199.
109. Saraswat, S.K.; Sinha, B.; Pant, K.K.; Gupta, R.B. Kinetic Study and Modeling of Homogeneous Thermocatalytic Decomposition of Methane over a Ni–Cu–Zn/Al $_2$ O $_3$ Catalyst for the Production of Hydrogen and Bamboo-Shaped Carbon Nanotubes. *Ind. Eng. Chem. Res.* **2016**, *55*, 11672–11680, doi:10.1021/acs.iecr.6b03145.

110. Levenspiel, O. *Chemical Reaction Engineering*; 3rd ed.; John Wiley & Sons, 1999; ISBN 0-471-25424-X.
111. Rodat, S.; Abanades, S.; Sans, J.-L.; Flamant, G. Hydrogen Production from Solar Thermal Dissociation of Natural Gas: Development of a 10kW Solar Chemical Reactor Prototype. *Solar Energy* **2009**, *83*, 1599–1610, doi:10.1016/j.solener.2009.05.010.
112. Rodat, S.; Abanades, S.; Coulie, J.; Flamant, G. Kinetic Modelling of Methane Decomposition in a Tubular Solar Reactor. *Chemical Engineering Journal* **2009**, *146*, 120–127, doi:10.1016/j.cej.2008.09.008.
113. Abanades, S.; Flamant, G. Hydrogen Production from Solar Thermal Dissociation of Methane in a High-Temperature Fluid-Wall Chemical Reactor. *Chemical Engineering and Processing: Process Intensification* **2008**, *47*, 490–498, doi:10.1016/j.cep.2007.01.006.
114. Paxman, D. Experimental and Theoretical Investigation of Solar Molten Media Methane Cracking for Hydrogen Production. M.Sc., University of Alberta: Department of Mechanical Engineering, 2014.
115. Paxman, D.; Trottier, S.; Flynn, M.R.; Kostiuk, L.; Secanell, M. Experimental and Numerical Analysis of a Methane Thermal Decomposition Reactor. *International Journal of Hydrogen Energy* **2017**, *42*, 25166–25184, doi:10.1016/j.ijhydene.2017.08.134.
116. Schindler, H.; Pastushenko, V.P.; Titulaer, U.M. A Measure for the Distance from Equilibrium. *Eur Biophys J* **1998**, *27*, 219–226, doi:10.1007/s002490050128.
117. Gosiewski, K.; Warmuzinski, K.; Tanczyk, M. Mathematical Simulation of WGS Membrane Reactor for Gas from Coal Gasification. *Catalysis Today* **2010**, *156*, 229–236, doi:10.1016/j.cattod.2010.02.031.
118. Plevan, M.; Geißler, T.; Abánades, A.; Mehravaran, K.; Rathnam, R.K.; Rubbia, C.; Salmieri, D.; Stoppel, L.; Stückrad, S.; Wetzel, Th. Thermal Cracking of Methane in a Liquid Metal Bubble Column Reactor: Experiments and Kinetic Analysis. *International Journal of Hydrogen Energy* **2015**, *40*, 8020–8033, doi:10.1016/j.ijhydene.2015.04.062.
119. Abanades, S.; Kimura, H.; Otsuka, H. Kinetic Investigation of Carbon-Catalyzed Methane Decomposition in a Thermogravimetric Solar Reactor. *International Journal of Hydrogen Energy* **2015**, *40*, 10744–10755, doi:10.1016/j.ijhydene.2015.07.023.
120. Abbas, H.F.; Daud, W.M.A.W. Deactivation of Palm Shell-Based Activated Carbon Catalyst Used for Hydrogen Production by Thermocatalytic Decomposition of Methane. *International Journal of Hydrogen Energy* **2009**, *34*, 6231–6241, doi:10.1016/j.ijhydene.2009.05.143.
121. Abbas, H.F.; Daud, W.M.A.W. Hydrogen Production by Thermocatalytic Decomposition of Methane Using a Fixed Bed Activated Carbon in a Pilot Scale Unit: Apparent Kinetic, Deactivation and Diffusional Limitation Studies. *International Journal of Hydrogen Energy* **2010**, *35*, 12268–12276, doi:10.1016/j.ijhydene.2010.08.036.
122. Mianowski, A.; Radko, T.; Siudyga, T. Influence of Initial Assumptions on the Kinetic Models of CO2 Gasification of Chars and Cokes in Solid Phase. *J Therm Anal Calorim* **2016**, *126*, 1911–1923, doi:10.1007/s10973-016-5660-y.
123. Msheik, M.; Rodat, S.; Abanades, S. CFD Simulation of a Hybrid Solar/Electric Reactor for Hydrogen and Carbon Production from Methane Cracking. *Fluids* **2023**, *8*, 18, doi:10.3390/fluids8010018.
124. Lente, G. Deterministic Kinetics in Chemistry and Systems Biology: The Dynamics of Complex Reaction Networks; SpringerBriefs in Molecular Science, 2014; ISBN 978-3-319-15482-4.
125. Meenakshi Sundaram, K. CATALYST EFFECTIVENESS FACTOR FOR LANGMUIR-HINSHELWOOD-HOUGEN-WATSON KINETIC EXPRESSIONS. *Chemical Engineering Communications* **1982**, *15*, 305–311, doi:10.1080/00986448208911076.
126. Douven, S.; Pirard, S.L.; Heyen, G.; Toye, D.; Pirard, J.-P. Kinetic Study of Double-Walled Carbon Nanotube Synthesis by Catalytic Chemical Vapour Deposition over an Fe-Mo/MgO Catalyst Using Methane as the Carbon Source. *Chemical Engineering Journal* **2011**, *175*, 396–407, doi:10.1016/j.cej.2011.08.066.
127. Starikov, E.B.; Nordén, B. Entropy–Enthalpy Compensation as a Fundamental Concept and Analysis Tool for Systematical Experimental Data. *Chemical Physics Letters* **2012**, *538*, 118–120, doi:10.1016/j.cplett.2012.04.028.